2017-10-01

Development and Testing of the Valence Multipole Model OH Potential For Use in Molecular Dynamics Simulation

Charles Stephen Andros
Brigham Young University

Development and Testing of the Valence Multipole Model OH Potential for Use in Molecular Dynamics Simulation

Charles Stephen Andros

A thesis submitted to the faculty of
Brigham Young University
in partial fulfillment of the requirements for the degree of

Master of Science

Barry Bickmore, Chair
Dean Wheeler
Thomas Knotts

Department of Geological Sciences

Brigham Young University

ABSTRACT

Development and Testing of the Valence Multipole Model OH Potential
for Use in Molecular Dynamics Simulation

Charles Stephen Andros
Department of Geological Sciences, BYU
Master of Science

Here we describe the fitting and testing, via molecular dynamics simulation, of a bond-order potential for water with a unique force field parameterization. Most potentials for water, including some bond-order (reactive) potentials, are based on a traditional, many-body decomposition to describe water's structure with bond stretch, angle bend, electrostatics, and non-bonded terms. Our model uses an expanded version of the Bond Valence Model, the Valence Multipole Model, to describe all aspects of molecular structure using multibody, bond-order terms. Prior work successfully related these multibody, bond order terms to energy, provided the structures were close to equilibrium. The success of this equilibrium energy model demonstrated the plausibility of adapting its parameterization to a molecular dynamics force field. Further, we present extensive testing of *ab initio* methods to show that the *ab initio* data we obtained, using the CCSD(t)/cc-pwCVTZ level of theory, to augment the fitting set of our parameters is of the highest quality currently available for the OH system. While the force field is not yet finished, the model has demonstrated remarkable improvement since its initial testing. The test results and the insights gleaned from them have brought us significantly closer to adapting our unique parametrization to a fully functional molecular dynamics force field. Once the water potential is finished, it is our intent to develop and expand the Valence Multipole Model into a fully reactive alternative to CLAYFF, a non-reactive potential typically used to simulate fluid interfaces with clays and other minerals.

Keywords: molecular dynamics simulation, bond-order potential, Bond Valence Model, Valence Multipole Model

ACKNOWLEDGMENTS

I would first like to thank my parents, for inspiring me since childhood to seek a Master's of Science degree. Without their love, support, and encouragement none of this work would have ever begun. I also wish to recognize the influence my siblings and closest friends have had on my work. The fun times that balanced the tough times, the laughs that helped me overcome the setbacks, and the inspiration they provided me that helped me persevere. Next, I wish to thank Dr. Barry Bickmore and Dr. Matthew Wander for the countless hours of help they provided me with. I wish to thank Dr. Wander specifically for the constant and invaluable assistance he provided me during these last several years. Finally, I want to thank Dr. Bickmore for the many years of mentorship and vision he has provided me, during both my undergraduate and graduate studies.

TABLE OF CONTENTS

LIST OF TABLES

LIST OF FIGURES

INTRODUCTION

In the field of computational chemistry, there is constant demand for more accurate, faster, and chemically reactive models. Molecular mechanics (MM) models, which describe atoms as "balls on springs," (Hinchliffe 2003) are specifically designed to meet the first two demands but are usually only accurate over a limited range of chemical scenarios. This limitation is especially evident when applying MM methods to model water, as demonstrated by the sheer number of water models in existence (Finney 2001,Guillot 2002). Attempts to improve these water models, like adding chemical reactivity, typically involve the addition of more adjustable parameters, which adds increased complexity and detracts from their computational efficiency.

Since the first rigid MM water model (Bernal and Fowler 1933), many improvements have been introduced to make them more realistic, such as adding interaction sites, flexibility, polarizability, and dissociability (Mahoney and Jorgensen 2000, H. Yu and Gunsteren 2003, Nada and Eerden 2003, Saint-Martin, Hess et al. 2004, Olano and Rick 2005, Wu, Tepper et al. 2006, Van Duin, Zou et al. 2014). To adequately simulate aqueous systems, however, a computationally efficient water model is necessary because large numbers of water molecules are required (Glättli, Daura et al. 2002, Horn, Swope et al. 2004). Therefore, rigid water models have emerged as the most popular. By holding strong H-O bonds and H-O-H angles rigid, the calculations become much more efficient. Additionally, most rigid water models use the assumption of "pair-wise additivity", which further improves their efficiency. This assumption states that each individual n-body interaction (u_{ij}) is completely independent of all other interactions and

that the sum of the energies of these interactions can be approximated as the total energy of the system (U_{total}):

$$U_{total} = \sum_{i<j} u_{ij} \quad (1)$$

(Rowley 1994). The simple point charge (SPC) SPC and transferable intermolecular potential (TIP) families of models are examples of rigid, and very popular, water models.

However, none of these rigid water models can ever satisfactorily reproduce all of water's physical and chemical behavior because they neglect anything involving the vibrational characteristics, polarizability, and reactivity of the molecules (Wallqvist and Berne 1993, Jorgensen and Jenson 1998, Van der Spoel, Van Maaren et al. 1998, Finney 2001, Guillot 2002, Ren and Ponder 2004, Mason and Brady 2007, Ball 2008, Tan, Cendagorta et al. 2014, Tan, Tran et al. 2016). Some have argued that water models do not need to reproduce all of water's behavior, but that rigid models need to be improved by including different data in the fitting set such as the temperature of maximum density (T_{md}) or the density of various ice polymorphs (Abascal and Vega 2005, Vega, McBride et al. 2005). Still others have proposed augmenting empirical data with, or even exclusively using, data obtained from *ab initio* methods (Burnham and Xantheas 2002, Xantheas 2005, Te and Ichiye 2010, Medders, Babin et al. 2014, Van Duin, Zou et al. 2014, Liu, Wang et al. 2016). Often, those employing *ab initio* data also advocate using dissociable water models, pointing out that only a dissociable water model can capture certain quantum and chemical effects, such as proton and hydroxyl ion transport. Furthermore, non-dissociable MM models will continually struggle to capture atomistic behavior at low temperature, because quantum effects become more pronounced, especially for light elements such as hydrogen (Billeter, King et al. 1994).

Historically, reactive water potentials have been less popular, in part due to their high computational expense. Reactive potentials are also very difficult to develop and expand because they have so many adjustable parameters, which multiply exponentially for each new atom type added to the force field. One approach for reducing the number of adjustable parameters is to augment a traditional MM force field with a bond order constraint. By introducing bond order to a traditional MM parameterization, the force field can account for the entire coordination sphere at once, thus avoiding the assumption of "pair-wise additivity". The ReaxFF force field is a good example of an arguably successful, reactive potential that augments a traditional MM parameterization with bond order (Van Duin, Baas et al. 1994, Van Duin, Dasgupta et al. 2001, Van Duin, Strachan et al. 2003, Van Duin, Zou et al. 2014). In addition to ReaxFF, several other bond-order potentials have been developed with reasonable degrees of success (Finnis and E. 1984, Tersoff 1988, Brenner 1990). However, despite using a traditional MM parameterization, bond-order potentials like ReaxFF still struggle with exponentially multiplying adjustable parameters. Thus, they typically cannot combine more than a select few elements into a single force field. We submit that restructuring the basic architecture of an MM force field can solve part of the parametrization issue. In this work, we explore a bond-order potential that uses a unique parameterization based almost entirely on bond valence, an empirical estimate of bond order using bond lengths.

Recently our group developed a bond-order potential that very accurately predicts the potential energy of structures near equilibrium for the element group Al, Si, O, and H (Wander and Bickmore 2016). Our use of bond valence in a bond-order potential is not without precedent (Grinberg, Cooper et al. 2002, Cooper, Grinberg et al. 2003, Grinberg,

Cooper et al. 2004, Shin, Cooper et al. 2005, Shin, Grinberg et al. 2007, Shin, Son et al. 2008, Grinberg, Shin et al. 2009, Liu, Grinberg et al. 2013, Liu, Grinberg et al. 2013, Takenaka, Grinberg et al. 2013). However, most bond-order potentials use bond order to correct the more traditional n-body terms (bond stretch, angle bend, etc.), the basic mathematical framework of our model is based on multi-body, bond-valence (i.e., bond-order) terms, with some more traditional terms added as correction. In other words, our force field is to our knowledge the first of its kind.

In this work, we describe part of the fitting and the initial testing of this new reactive potential for water. One challenge faced while fitting the model was a lack of adequate data with which to fit our reactive potential. Non-reactive potentials are typically fitted to macroscopic, physical properties (atom pair radial distribution functions, T_{md}, etc.). However, this choice of calibration data is insufficient for developing a reactive water potential, where transition states need to be described in detail. Due to recent advancements in *ab initio* methods, *ab initio* data is increasingly used both for fitting model parameters and/or examining a model's behavior around transition states (Van Duin, Baas et al. 1994, Van Duin, Dasgupta et al. 2001, Van Duin, Strachan et al. 2003, Ren and Ponder 2004, Xantheas 2005, Te and Ichiye 2010, Medders, Babin et al. 2014, Tan, Cendagorta et al. 2014, Van Duin, Zou et al. 2014, Liu, Wang et al. 2016, Tan, Tran et al. 2016). However, different *ab initio* methods exhibit varying degrees of accuracy with respect to various quantum properties. We therefore decided to first test a wide range of *ab initio* methods to determine a level of theory that was sufficiently accurate for our purposes (see Appendix – Tables 1 and 2). We ultimately used the CCSD(t) level of theory with the cc-pwCVTZ (correlation consistent,

polarization, weighted, core and valence, triple zeta) basis set to calculate various oxygen and hydrogen configurations to augment our calibration dataset (see Appendix – Tables 3 and 4).

Once the model parameters were calibrated, we determined to test our water model by simulating five macroscopic properties of water. The five selected properties are (in order of importance): atom pair radial distribution functions (RDF), self-diffusion coefficient, temperature of maximum density (T_{md}), and the thermal expansion coefficient (expansivity) and isothermal compressibility at different temperatures. Most agree that a reliable water potential needs to reproduce experimental values for all atom pair RDFs and the self-diffusion coefficient at room temperature. The T_{md} is a unique property of water derived from the hydrogen bonding network that water forms. We therefore reasoned our model should be able to reproduce the T_{md} since one of the great strengths of bond valence is accounting for complex bonding networks. The expansivity and compressibility tests were selected because these are easily derived from a T_{md} calculation.

Our goal for this water potential is to develop a reactive alternative to the MM force field CLAYFF (Cygan, Liang et al. 2004). CLAYFF is a nonreactive potential designed to simulate fluid interfaces with clays and other minerals characterized by complex and disordered structures and composition. The first step towards developing a reactive version of CLAYFF is to develop a potential for the OH system. Once the OH potential is developed, we will expand the potential to include those elements necessary to simulate clays (Si, Na, K, Cl, etc.).

THEORY

All MM force fields require three essential components: structural descriptors, ideal values for those structural descriptors and energy cost functions for deviation from said ideal values. Many energy cost functions are similar to Hooke's Law for springs,

$$u = \frac{1}{2}k(x - x_0)^2 \quad (2)$$

Here, the spring length x is the structural descriptor, u describes the energy cost in terms of potential energy, x_0 is the ideal value of the structural descriptor, and k is a constant. Most MM force fields have multiple energy cost functions with one or more structural descriptors that can be adjusted to fit some set of data including thermodynamic data, physical properties, and crystal/molecular structures (Rappé and Casewit 1997, Hinchliffe 2003, Cramer 2004, Comba, Hambley et al. 2009). Except for Van der Waals and traditional electrostatics terms for non-bonded atoms, all the structural descriptors in our model are based on bond valence.

Bond Valence and the Bond Valence Model

The concept of bond valence grew out of Pauling's treatment of oxidation number, or atomic valence (V_i), as a measure of the atom's bonding power, which is distributed as bond valence in all bonds incident to the central atom (Pauling 1929). Bond valence is typically calculated using a simple exponential function (Eqn. 3) or power function (Eqn. 4) to relate the interatomic distance between ions i and j (R_{ij}) to bond valence (s_{ij}).

$$|s_{ij}| = e^{(R_0 - R_{ij})/B} \quad (3)$$

$$|s_{ij}| = \left(\frac{R_0}{R_{ij}}\right)^{1/B} \quad (4)$$

Both R_0 and B are fitted empirical parameters specific to a given atom pair, where R_0 is the bond length at which s_{ij} = 1 in valence units (v.u.) and B describes the curvature of the function (Brown and Altermatt 1985).

As mentioned previously, all MM models require three essential components: structural descriptors, ideal values for those structural descriptors, and energy cost functions. The BVM exhibits two of these essential components (see below) but does not use an energy cost function. The structural descriptor of the BVM is the bond valence sum (S_i).

$$S_i = \sum_j s_{ij} \quad (5)$$

The first axiom of the BVM, the "valence sum rule," states that the valence sum is ideally equal to the atomic valence (Brown 2002, Wander, Bickmore et al. 2015).

$$\sum_j s_{ij} \approx V_i \quad (6)$$

In this way, the valence sum rule can be thought of as defining the ideal value of the $S_i$structural descriptor. A structure may be stable if the valence sum rule is closely followed, which implies an energy cost for deviation, but no specific function is used to describe it. The atomic valence is equal to the absolute value of the oxidation state if only polar bonds are considered (Brown 2002, Wander, Bickmore et al. 2015). For example, the ion O^{2-} has an atomic valence of 2 v.u. In the $H_2O_{(g)}$ molecule, the O^{2-} forms two polar O-H bonds each with ~1.0 v.u. Therefore, the sum of the bond valences reaching the central O is 2 v.u., or its atomic valence.

To develop a force field based mostly on bond valence, we have performed several expansions of the BVM. These expansions are as follows: development of several new bond valence-based structural descriptors using a multipole expansion, accounting

for fully covalent bonds, and redefining and optimizing the shape of bond valence curves to produce appropriate potential energy surfaces. This expanded model, still under development, is called the Valence Multipole Model (VMM) (Wander and Bickmore 2016).

Valence Multipole Model

Because the improvements to the VMM are still on-going, we present the current stages of development in four separate phases. First, we show the expansions made to the original BVM to create structural descriptors for the VMM. Second, we present the VMM as an equilibrium energy model, which demonstrates it is possible to develop robust ideal values and energy cost functions for the structural descriptors of the VMM. Third, we examine the adjustments made to the functions and parameters of the equilibrium model to make it a fully reactive potential for the OH system. This reactive potential was designed to account for much of the complex quantum behavior exhibited by the OH system. We did this knowing that simplification of the model would likely be necessary, instead the objective of this procedure was to see how much complexity we could initially incorporate into the potential. The tests presented later in this work explore the strengths, weaknesses, and key issues associated with this new reactive potential. Finally, we discuss some of the simplifications we introduced to the model in accordance with the test results. These simplifications are designed to help bring our potential closer to functioning properly as a fully reactive molecular dyanmics force field.

Expanding the BVM

The first expansion of the BVM involved developing bond-valence parameters for same-ion types. The traditional BVM addresses polar covalent and ionic bonds but does

not address fully covalent bonds. Wander et al. (2015) showed that for the Al-Si-K-O and Al-Si-H-O systems, inclusion of anion-anion bonding in calculating the bond valence sum produced significant improvements in the adherence of known structures to the valence sum rule. In addition to improving the bond valence sum, allowing for same-ion interactions permits the model to account for co-ion attractive and repulsive interactions using bond valence. For example, $H_2O_{2(g)}$ forms two bonds, one polar O-H bond and one fully covalent O-O bond. Instead of assuming an atomic valence of 1 for O^{1-}, i.e., the absolute value of its oxidation state, we assume an atomic valence of 2. Thus, we have 1 polar O-H bond with ~ 1.0 v.u. and one covalent O-O bond with ~1.0 v.u (Wander, Bickmore et al. 2015).

The second expansion of the BVM was redefining and optimizing the bond valence-length curve relationships to account for a wide range of bond lengths, such as would be required to describe transition states. The BVM is traditionally used to determine the plausibility of proposed crystal structures, therefore the bond valence-length curves were originally calibrated on crystal structure data. This is problematic because crystal structures typically display a very limited range of bond lengths. Wander et al (2015) used both molecular and crystal structure data to show that neither Eqn. 3 nor 4 is flexible enough to capture the bond valence-length relationship over a large distribution of bond lengths. They therefore developed a series of more flexible, hybrid power-exponential functions, with 3 (Eqn. 7) and 4 (Eqn. 8) fitted parameters respectively:

$$s_{ij} = e^{(R_0 - R_{ij})w/B} \left(\frac{R_0}{R_{ij}}\right)^{(1-w)/B} \quad (7)$$

$$s_{ij} = we^{(R_0 - R_{ij})/B_1} + (1-w)e^{(R_0 - R_{ij})/B_2} \quad (8)$$

Here, s_{ij} is the bond valence in valence units (v.u.), R_{ij} is the bond length between atoms i and j, B and R_0 are fitted parameters, and w is a weighting parameter. These new equations were much better suited to describing the bond valence-length relationship over a wide range of bond lengths.

The third expansion of the BVM involved the development of new bond valence-based structural descriptors. The BVM, despite its inherent strength for identifying plausible combinations of bond lengths, cannot address some other aspects of molecular structure, such as the angular distribution of bonds. To remedy this, we performed a multipole expansion of the bond valence incident to individual atoms out to the quadrupole moment. We accomplished this by treating bond valences as vector quantities in the direction of the bond, with magnitude equal to the bond valence. These new structural descriptors allow us to describe all aspects of molecular structure using fully multibody terms. The monopole moment of the multipole expansion is provided by the bond valence sum. The dipole moment structural descriptor is the norm of sum of the bond valence vectors and describes the lopsidedness of the bond valence distribution (Bickmore, Wander et al. 2013). The quadrupole moment descriptor is provided by the Frobenius norm of a second-order tensor that describes the ellipsoidal distribution of the bond valence. The dipole moment can describe non-centrosymmetric distortions, while the quadrupole moment describes centrosymmetric distortions, such as caused by Jahn-Teller effects (Shepherd, Wander et al. 2016).

Equilibrium Energy Model

Wander and Bickmore (2016) developed ideal values and energy cost functions for the new structural descriptors of the VMM for the element group Al-Si-H-O.

Provided that the bond valence sum was within 0.2 v.u. of the atomic valence, or rather for stable structures at equilibrium, the model provided accuracies of ~5 kJ/mol per unique atom, which is comparable to some *ab initio* approaches. The energy cost function for the valence monopole structural descriptor was computed using a Morse-like potential:

$$E_{VM,i} = \frac{1}{2} V_i D_{E1,i} \left(\left(\frac{S_i}{V_i} \right)^{\alpha_i} - 1 \right)^2 \quad (9)$$

Here, $E_{VM,i}$ is the valence monopole energy for atom i. $D_{E1,i}$ is a weighted average of the dissociation energies of all bonds incident to atom i and is analogous to the well depth term in a Morse potential, S_i is the bond valence sum, and V_i is the atomic valence. The α_i term is discussed in further detail below. The energy cost function of the valence dipole descriptor was a simple harmonic function:

$$E_{VD,i} = k_{VD,i} \left(\left\| \vec{P_i} \right\| - \left\| \vec{P_i} \right\|_{Ideal} \right)^2 \quad (10)$$

Where $k_{VD,i}$ is a kind of spring constant and $\left\| \vec{P_i} \right\|$ the norm of the sum of the bond valence vectors. For water, there is only one defined value of $\left\| \vec{P_i} \right\|_{Ideal}$, which is designed to produce an HOH bond angle of 104°. A similar treatment was used for the valence quadrupole energy cost function, but because it is not relevant to this work is it not discussed in further detail here.

The α_i parameter in Eqn. 10 is a function of the averaged bond force constant ($k_{1,i}$), the well depth term ($D_{E1,i}$), and the averaged bond valence curvature parameter (B_i) and was computed as follows:

$$\alpha_i = B_i \sqrt{\frac{k_{1,i}}{2D_{E1,i}}} \quad (11)$$

To compute the averaged force constant $k_{1,i}$, they used prior work to show there exists a linear relationship between a bond's force constant and its bond order (Badger 1934, Johnston 1966). They therefore calculated an individual bond's force constant using the following equation:

$$s_{ij} = \frac{k_{1,ij}}{k_1} \tag{12}$$

Where k_1 is the force constant of a single bond and $k_{1,ij}$ is the force constant for the single bond between atoms i and j. However, because the bond valence is inherently a multibody parameter, values that are typically associated with a particular bond need to be averaged over all bonds incident to the central atom. Therefore, they used a weighed arithmetic mean over all incident bonds ij to obtain $k_{1,i}$ as well as the averaged values $D_{E1,i}$ and B_i:

$$k_{1,i} = \left(\frac{1}{S_i}\sum_j s_{ij}k_{1,ij}\right) \tag{13}$$

$$D_{E1,i} = \left(\frac{1}{S_i}\sum_j s_{ij}D_{E,ij}\right) \tag{14}$$

$$\frac{1}{B_i} = \left(\frac{1}{S_i}\sum_j \frac{s_{ij}}{B_{ij}}\right) \tag{15}$$

Here, B_{ij} is the same as the function curvature B parameter seen in Eqn. 7. In cases where Eqn. 8 was needed, two different bonds are computed using each of the B_1 and B_2 parameters.

The final parameter, $D_{E,ij}$, was estimated using a polynomial function of s_{ij}. For most atom pairs in the Al-Si-H-O element group, the following function was adequate to relate the dissociation energy of a bond ($D_{E,ij}$) to the bond valence:

$$D_{E,ij} = as_{ij} + bs_{ij}^2 + \cdots \tag{16}$$

However, O-H bonds were an exception and required a slightly different functional form:

$$D_{E,ij} = as_{ij}^{1/2} + bs_{ij}^{c} \quad (17)$$

In both Eqn. 16 and 17, a, b, c, etc., are fitted constants.

The Initial Reactive OH Potential

Wander and Bickmore (2016) noted that further work would be required to calibrate the model to describe transition state configurations. Wander et al (*in prep*) used a database of *ab initio* calculations (see Appendix – Tables 3 and 4) to refit the model parameters of Wander and Bickmore (2016) to develop a model for use in molecular dynamics (MD) simulation for the O-H group. Furthermore, valence monopole energy cost function and parameters had to be slightly repurposed so they could be integrated in real time. Wander et al (*in prep*) did this by making the key valence monopole parameters (D_E, k, ands_{ij}) a function of a new parameter s_{min}, which is s_{ij} defined at the minimum energy. This defined a new triad of valence monopole parameters (D_e, F, and R_{min}). Now, the valence monopole energy is calculated as the sum of the bonds incident to it,

$$E_{VMM} = \frac{1}{2}\sum_j E_{ij} \quad (18)$$

and the energy of the bond between atoms ij is a Morse-like function defined as,

$$E_{ij} = e^{-2\alpha\left(R_{ij}-R_{min}(s_{min})\right)} - 2e^{-\alpha\left(R_{ij}-R_{min}(s_{min})\right)} \quad (19)$$

where,

$$\alpha = \sqrt{\frac{F(s_{min})}{2D_e(s_{min})}} \quad (20)$$

According to this formulation, each bond only receives half of the energy of the bond. This specification is necessary to account for structures, like ozone, where two atoms prefer different bond orders.

Wander et al (*in prep*) further had to develop a formulation for each component of the new valence monopole triad (D_e, F, and R_{min}). For the force constant (F), the formulation is very similar to the original,

$$F(s_{min}) = F_{single} s_{min} \quad (21)$$

where F_{single} is the force constant of a single bond. The dissociation energy (D_e) required more adjustment. Continued work showed the polynomial functional form (Eqn. 17) was insufficient to describe the relationship between s_{ij} and D_e at large bond orders. So instead Wander et al. (*in prep*) used a logistic functional form,

$$D_e = \frac{L}{1+e^{-k(s_{min})}} + \sum_n \frac{L_n}{1+e^{-k_n(s_{min}-s_{0n})}} - D_e(s_{min} = 0) \quad (22)$$

where L, k, and s_0 are fitted parameters. For R_{min}, which is the bond length between atoms ij at s_{min}, they numerically inverted Eqn. 8 to obtain the following equation,

$$R_{min} = c_0 + \sum_n c_n e^{(a_n - s_{min})/b_n} \quad (23)$$

This numerical differentiation is correct to within 0.001 Å.

Because the ideal value of s_{min} is inherently dependent on the instantaneous chemical environment in which a given atom finds itself, Wander et al (*in prep*) faced some difficulty finding the proper value of s_{min}. As they explored different methods for defining s_{min}, they noted that V_i, the atomic valence, changed as a function of the coordination number. They therefore defined s_{min} as a function of coordination number (N_{coord}),

$$S_{min} = \frac{V_i}{N_{coord}} \quad (24)$$

The coordination number is therefore calculated at every time step as a function of the instantaneous bond valences and the bond valence sum,

$$N_{coord} = \frac{S_i^2}{\sum_j s_{ij}^2} \quad (25)$$

Further, to ensure the coordination number is always an integer value, we added a rounding function to Eqn. 25. Thus, Eqn. 25 allows the s_{min} of each bond to be updated at every time step, providing a new set of values for the valence monopole triad (D_e, F, and R_{min}).

Finally, to account for non-bonded interactions, Wander et al (*in prep*) introduced a method to describe repulsion between ions of the same type. Bonding between ions of the same type, such as two O^{2-} ions, is assumed to be negligible. So, we introduced a pairwise, non-bonded term called the Morse-cut potential,

$$E_{ij,i} = D_{NB,i}\left(e^{-2\alpha\left(R_{ij}-R_{min}(s_{min})\right)} - 1\right)^2 + D_{NB,i} \quad (26)$$

Here $D_{NB,i}$ is the dissociation energy of the repulsive potential energy curve for a given co-ion pair. The Morse-cut potential can be thought of as a core-core repulsion term and is responsible for ensuring atom pairs do not approach each other too closely. The Morse-cut potential makes use of a cutoff radius where $R_{cut} = R_{min}$ for the atom pair and outside the cutoff radius, the Morse-cut potential is set to 0. However, to prevent the Morse-cut potential from operating on ions within a molecule, we added a 1-3 bonding term. The following equation defines the criteria for a "bound" atom,

$$s_{ij} \geq \frac{V_i}{2N_{coord}} \quad (27)$$

This allows the model to consider ions within a molecule as "bonded" and thus not subject to the Morse-cut potential.

Refining the Reactive OH Potential

The functional forms of the O-H potential discussed above were subjected to rigorous tests, discussed below. The test results revealed a very important issue intrinsic to the framework of the VMM: it allows too much structural flexibility. Traditional MD force fields, which assume pairwise additivity, excel at constraining atomistic behavior such that certain physical properties are precisely reproduced when subject to the appropriate conditions. The current multi-body terms of the VMM OH potential (valence monopole and dipole) avoid pairwise additivity but allow too much structural flexibility. We therefore performed a series of adjustments to the VMM OH potential to constrain its behavior.

The most significant manifestation of excess flexibility in the model was the ability to bond a hydrogen atom to two oxygen atoms. Due to energy conservation issues within the model potential itself (see below), atoms attained very high kinetic energy values during MD simulation. This allowed non-bonded hydrogen atoms to come very close to the proximal oxygens. Once a non-bonded hydrogen came within about 1.4 Å of a neighboring oxygen, the N_{coord} (Eqn. 25) of that oxygen increased from 2 to 3, allowing the previously weak O-H to become a strong O-H bond. This was problematic as it allowed the hydrogen to become fully bonded to two proximal oxygens. The solution was defining an "excess" s_{ij}, which is always greater than or equal to zero.

$$s_{ij,excess} = minimum(S_i - V_i, S_j - V_j) \tag{28}$$

The $s_{ij,excess}$ is used to determine the corrected bond valence value,

$$s_{ij}{}' = s_{ij} - s_{ij,excess} \tag{29}$$

Here s_{ij}' is the bond valence corrected for over-bonding. Next, we extended the pairwise, repulsive Morse-cut potential (Eqn. 26) to include non-bonded O^{2-} and H^{+} ions. This means that the only non-bonded, attractive potential present in the VMM is the Coulombic potential. Finally, to help simplify the model, we decided to remove the soft-core Coulombic potential and replace it with a traditional Coulombic potential,

$$E_{coul} = \frac{Cq_iq_j}{\epsilon r} \tag{30}$$

Where C is a conversion constant, q is the charge on atoms i and j, ϵ is the dielectric constant and r is the interatomic distance.

Model Calibration

All ab initio calculations used for fitting the model parameters were performed using the CCSD(t) level of theory with the cc-pwCVTZ basis set. CCSD(t) indicates a full treatment is provided for singlet and doublet states and perturbation theory is used to approximate the triplet states. These excited states (singlet through triplet) are sometimes considered necessary to obtain accurate energies (Cramer 2004). Some have even asserted that the CCSD(t) level of theory, combined with the cc-pCVnZ basis sets, should provide sufficiently accurate water cluster data for fitting a reactive water model (Xantheas 2005).

The correlation-consistent family of basis sets (cc-pVnZ) was developed with the intent of approximating the complete basis set, which hypothetically gives the exact solution to the Schrödinger equation within the limits of that basis set and within the Born-Oppenheimer approximation (Balabanov and Peterson 2005). In most calculations, the frozen core approximation (which neglects electron correlation of core electrons) is acceptable to use. However, in cases where highly accurate thermodynamic properties or

geometries are required, the electron correlation with the core electrons cannot be ignored. Therefore, the cc-pCVnZ basis sets were specifically designed to handle the core-valence correlation (Peterson and Dunning 2002, Peterson and Puzzarini 2005). Peterson and Dunning (2002) further tested and developed a set of weighted correlation consistent, core-valence basis sets (cc-pwCVnZ). The weighted basis sets weigh the core-valence electron correlation more heavily than the core-core correlation. Like the unweighted basis set family cc-pCVnZ, the weighted basis sets demonstrated superior convergence to empirical molecular property values. However, they recommended that when considering energetic or spectroscopic properties the weighted basis sets should be used over the unweighted basis sets. They further provided dissociation energies and bond lengths for several oxygenated species obtained using the cc-pwCV(T,Q)Z basis sets that were highly accurate.

Soft-Core Electrostatics

The structural descriptors of the initial VMM OH potential were calibrated on equilibrium structures and thus designed to handle short-range interactions. However, when performing MD simulation long-range interactions play a key role in the structuring of the molecules. Therefore, it became necessary to introduce a traditional Coulombic potential to the VMM force field. The soft-core electrostatics potential was developed for use in conjunction with a second potential that accounts for short-range interactions and was therefore highly desirable for the VMM water model. By using the soft-core Coulombic potential, the model can use exclusively bond-valence to handle short-range interactions and a traditional Coulombic potential for long-range interactions.

The soft-core electrostatics potential (known in LAMMPS as the pair style coul/long/soft) was developed to avoid singularities or numerical instabilities, which occur during free energy calculations when sites are created or removed (Beutler, Mark et al. 1994). The Coulombic energy is calculated using the following equation:

$$E = \lambda^n \frac{Cq_iq_j}{\varepsilon[\alpha(1-\lambda)^2+r^2]^{\frac{1}{2}}} \text{ for } r < r_c \quad (31)$$

Where C is a conversion constant, q_i and q_j are the charges of atoms ij, ϵ is the dielectric coefficient, r is the interatomic distance, n and α are positive constants and λ is the activation parameter. When $\lambda = 1$, the electrostatic interactions are calculated as a traditional Coulombic potential with a cutoff. When $\lambda = 0$, the electrostatic interactions are ignored. While the use of soft-core electrostatics with the VMM has been deprecated, this potential was present in all MD simulations described below.

METHODS

To determine the most accurate and efficient method for the *ab initio* calculations, we performed a series of geometry optimizations of Na_2 using the CCSD, CCSDT, CCSD(t) and configuration interaction with doublets (CID) theories. We tested each level of theory in conjunction with the correlation consistent basis sets: cc-pVnZ, cc-pCVnZ. All the basis sets were tested with double, triple, quadruple and, in some cases, quintuple zeta. We also tested both the augmented and non-augmented versions of these basis sets using CCSD. The total number of Na_2 geometry optimization tests used to determine the optimal level of theory was 55 optimizations (Appendix – Table 1). We then proceeded to perform 9 bond energy scans of Na_2 using the cc-pCV(D,T,Q)Z basis sets and the CCSD, CCSD(t) and CCSDT levels of theory (Appendix – Table 2). All *ab initio* calculations were performed using the Gaussian 09 software.

The combination of CCSD(t) with cc-pwCVTZ was used for all *ab initio* calculations used to augment the database used to fit the model parameters. A total of 29 oxygen and hydrogen species were calculated and included in the data fitting set (Appendix – Tables 3 and 4). The species were selected to give as wide a spread of bond valences as possible so that our fitting set accounted for most plausible bond valences.

The molecular dynamics software package LAMMPS was used to perform all molecular dynamics tests of the VMM water model. The initial configuration for all VMM water simulation tests was a 15.56 x 15.56 x 15.56 Å proton-disordered ice (Ih) crystal with 128 water molecules. The NVT ensemble (constant number of particles, volume and temperature) was used for most MD simulations. The NVE ensemble (constant number of particles, volume and energy) was used to measure the model's energy conservation. The temperature for all simulations performed in NVT was maintained by velocity scaling. Simulation temperatures were reached by scaling up from zero to the desired temperature over 1 picosecond (ps). A time-step of 0.1 femtosecond was used to help ensure energy conservation. All simulations were run on a total of 16 processors and achieved close to 100 ps of simulation time. For the soft-core electrostatic potential (LAMMPS pair style coul/long/soft), a λ of 0.99 and n of 1 were used. A Coulombic potential cutoff of 7.5 Å was used. We varied the α parameter to determine the optimal value for VMM water simulation. The Ewald summation technique was employed for long-range electrostatic interactions (Ewald 1921).

The properties of maximum density, compressibility and expansivity are typically simulated using the NPT ensemble (constant number of particles, pressure and temperature) at atmospheric pressure. We decided to perform these tests by running

multiple simulations in NVT and adjusting the volume of the box at the start of the simulation and allowing the box to equilibrate. We tested this methodology using the TIP4P/2005 potential and obtained a linear relationship between density and pressure at a variety of temperatures. This relationship gave the water's density under the conditions of atmospheric pressure and the box temperature. Using these density values, we reproduced very well the temperature of maximum density (T_{md}) and the expansivity and compressibility values at those temperatures.

RESULTS AND DISCUSSION

We first discuss the results from our tests of *ab initio* methods and the oxygen and hydrogen species we used to augment our parameter fitting database. Next, we present the VMM's MD simulated values for unit pair RDFs, diffusivity and T_{md}. The unit pair RDFs revealed the water structure was incorrect. On-going work suggests this may be caused by the valence dipole moment insufficiently constraining the HOH bond angles. Further, the values obtained for T_{md} and diffusivity suggested that the gradients of the VMM were not being properly calculated, so we performed an MD simulation using the NVE ensemble. This simulation confirmed that the VMM gradients were being improperly calculated, as demonstrated by periods of substantial energy gain and steady temperature increase during the simulation. Consequently, we began searching for discontinuities in the VMM's valence monopole and dipole potentials. We found and resolved one discontinuity in the valence monopole potential but the model still does not conserve energy during MD simulation. We suspect the remaining problem yet lies in transitions between allowed ideal states of the valence monopole and dipole moments.

There are many ideal states allowed and we have yet to account for the model's behavior during transitions between all ideal states.

Ab Initio Calculations

The results from the Na_2 *ab initio* calculations were used to determine what level of *ab initio* was accurate enough to augment our calibration data set. Examination of the Na_2 molecule geometry optimizations revealed the cc-pCVnZ family of basis sets were the most consistently correct across all levels of theory (Appendix – Table 1). To determine exactly what level of theory and basis set we should use, we performed bond dissociation scans on Na_2 molecules (Appendix – Table 2). The values calculated in these bond scans included bond length (R), dissociation energy (De) and force constant (k). Ultimately, we determined the CCSD(t) level of theory combined with the cc-pCVTZ basis set was the best combination of efficiency and accuracy for Na_2. However, since *ab initio* calculations perform differently for different elements, we examined the results from Peterson and Dunning (2002) who performed calculations using oxygenated species with both the cc-pCVTZ and cc-pwCVTZ basis sets. They ultimately recommended the cc-pwCVnZ basis sets over cc-pCVnZ basis sets.

We therefore used the CCSD(t)/cc-pwCVTZ level of theory to examine oxygen-oxygen and hydrogen-oxygen bonds over a spread of bond valence values. It is noteworthy to mention that some of the species included in the fitting set were unusual radicals, however these structures were necessary to provide a good sampling of bond valences (see Appendix – Table 3 and 4). Furthermore, because we have thoroughly tested our selected level of theory, we are confident the values obtained from these structures are sufficiently accurate.

MD Simulation Tests

Here we present the MD simulated values for all oxygen-hydrogen unit pair radial distribution functions (RDF), the self-diffusion coefficient and the temperature of maximum density (T_{md}). Because the T_{md} test failed, we were unable to calculate the expansivity and compressibility values. All MD simulated values demonstrated poor agreement with experimental values. We initially thought this shortcoming indicated our simulation conditions and/or the soft-core Coulombic potential parameters were improperly assigned. However, experimentation with the Coulombic potential parameters and the simulation conditions yielded no significant improvement. This led to the hypothesis that the T_{md} and self-diffusion coefficient values were erroneous because VMM OH potential's gradients were being improperly calculated.

Radial Distribution Functions

RDFs for the oxygen-oxygen, oxygen-hydrogen and hydrogen-hydrogen atom pairs were computed and compared with experimental values (Figures 1 – 3). Please note that the experimental RDFs did not account for bonded atoms. All RDFs were computed at close to 300 K with a box density of 1.02 g/cm^3. The RDFs reveal that the water structure predicted by the model is flawed: all RDFs have either missing peaks and/or structural abnormalities.

At first, we believed the structural abnormalities were caused by improperly combining the soft-core electrostatic potential with the bond valence potentials. We therefore varied the α parameter of the Coulombic potential to produce different radii of curvature for the short-range portion of the Coulombic potential's curve. We computed RDFs using eight different alpha values, varying the curvature of the Coulombic potential

curve from nearly flat to a traditional Coulombic potential curve. Little to no difference was noted between the eight sets of RDFs. The RDFs presented here were calculated using a Coulombic potential curve with the largest tested radius of curvature (i.e., a nearly flat Coulombic potential curve).

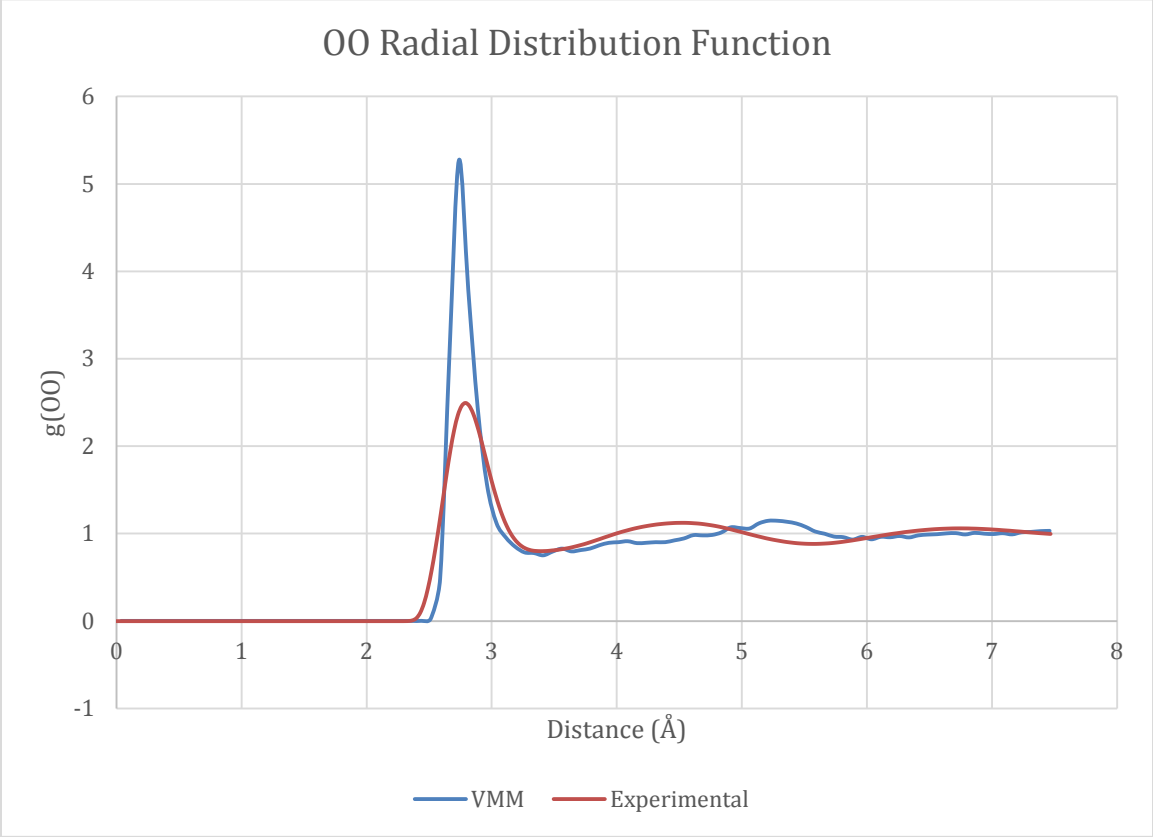

Figure 1 – Comparison of the VMM MD simulated and experimental oxygen-oxygen unit pair radial distribution functions. Note the lack of O-O structure past 3 Å.

The first peak in the OO RDF (Figure 1) at 2.8 Å is too tall and sharp, suggesting perhaps the gradients of the oxygen-oxygen either the repulsive or the attractive potential may be slightly too steep. However, comparatively speaking, the sharpness of the first peak is not unusual for an MD force field. Looking at the second peak, the experimental RDF demonstrates a broad peak centered at about 4.5 Å. The VMM's second peak however is rather sharp and close to 5.5 Å. It is possible the VMM's peak at 5.5 Å is merely the second peak shifted, or it could be an entirely different and fictitious structure.

The second peak of the OH RDF (Figure 2) at 1.9 A is too steep and narrow, suggesting again that the gradients for bonded O-H pairs are too steep. The third peak occurs at about the right distance, 3.1 Å, but it is too wide and slightly deformed, which suggests some unusual O-H structuring is occurring around 3.5 Å.

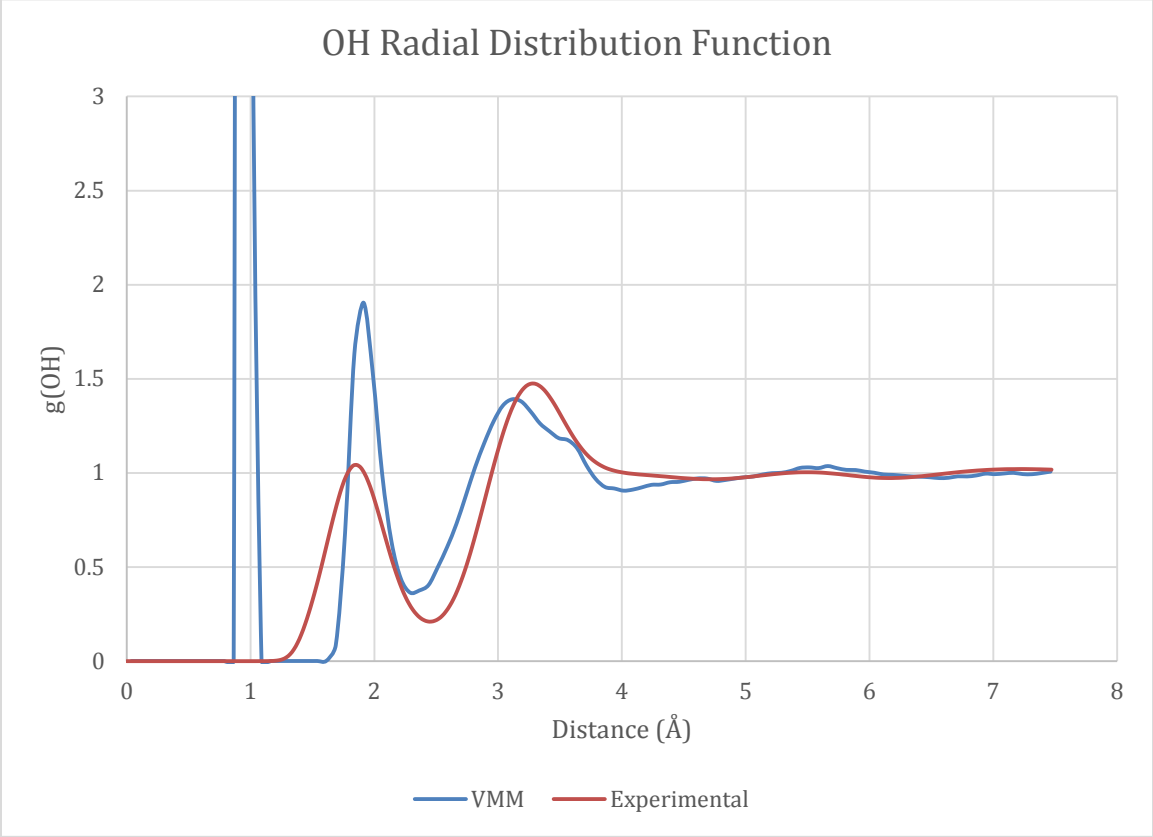

Figure 2 – Comparison of the VMM MD simulated and experimental oxygen-hydrogen unit pair radial distribution functions. The first peak is bonded structures. Note the unusual O-H structuring around 3.5 Å.

The first peak of the HH RDF is very wide (Figure 3), suggesting that the model allows hydrogen atoms to come into proximity to each other. Visualization of the molecules during MD simulation indicated that the hydrogens on neighboring water molecules were oriented towards each other instead of the oxygens. Further, a wide spread of HOH bond angles was observed during the simulations. These erroneous behaviors are probably what caused the width of the first peak.

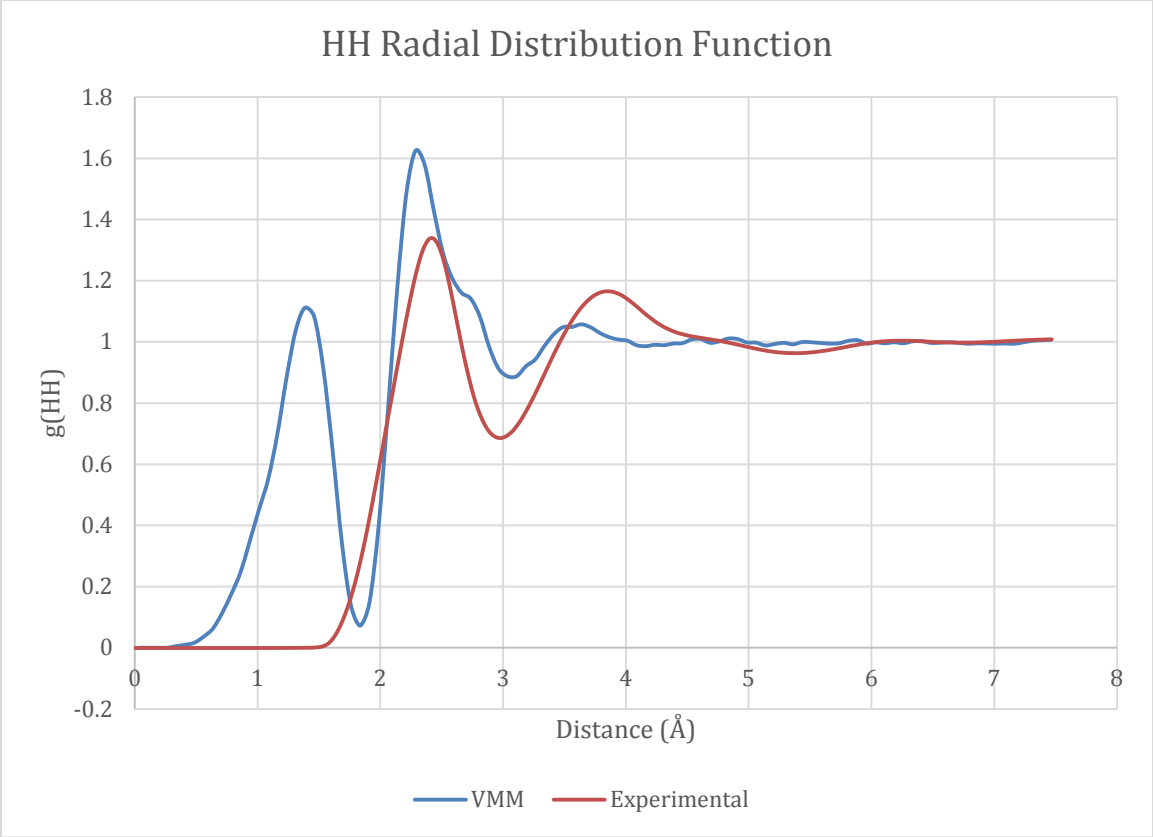

Figure 3 – Comparison of the VMM MD simulated and experimental hydrogen-hydrogen unit pair radial distribution functions. Note the wide first peak.

Self-Diffusion Coefficient

For the self-diffusion coefficient, we first obtained self-diffusion coefficients from the models TIP4P/2005, SPC-E and ReaxFF to ensure our methodology was correct. The simulated self-diffusion coefficients were all within 6% of the literature values (Table 1).

Model	$D*10^{-9}$ (m^2/s)	
	Simulated	Literature
VMM	714	-
SPC/E	2.65	2.49
TIP4P/2005	1.95	2.08
ReaxFF	2.06	2.11
Experiment	-	2.27

Table 1 – Reproduced water self-diffusion coefficients with the VMM's self-diffusion coefficient at 298 K. The literature value for SPC-E was taken from *(Chaplin 2001)*. The experimental and TIP4P/2005 values were taken from Abascal and Vega (2005). The ReaxFF value was simulated using the Fe/O/water parameter file *(Aryanpour, van Duin et al. 2010)* and the literature value taken from Adri et al. (2013).

We calculated the self-diffusion coefficient using the Einstein equation

$$6Dt = \lim_{t \to \infty}(|r_i(t) - r_i(0)|)^2, \quad (32)$$

where $r_i(t)$ is the position of particle i at time t. The VMM self-diffusion coefficient in Table 1 is wildly inaccurate and is more representative of a gas-phase self-diffusion coefficient. Furthermore, velocities had to be rescaled every five time-steps to prevent the simulation temperature from rapidly climbing.

Initially, as with the RDFs, we thought the erroneous behavior was caused by improperly combining the short-range bond valence potentials and the soft-core Coulombic potential. We tested this by varying the charge of the oxygen from -0.6 to -1.0 *e*, in five increments of 0.1 *e*, and the Coulombic potential's radius of curvature from 3 to 7 Å, in five increments of 1 Å, for a total of 25 simulations. We further examined a simulation with no charge, which removed all long-range interactions from the model. Ultimately, the variation in the self-diffusion coefficient in the charged tests was negligible. The uncharged simulation produced a noticeably different value for the self-diffusion coefficient but it was still representative of a gas-phase diffusivity. These results demonstrated that charge was not the determining factor for the gas phase-like self-diffusion coefficient. We therefore decided to use a charge of -0.7 *e* for oxygen and 0.35 *e* for hydrogen because this produces a charge dipole very close to the correct dipole for liquid water.

Because charge had a negligible effect on the self-diffusion, we questioned whether the simulations adequately conserved energy. We decided to test different length time steps to see if a smaller time step would produce a more realistic self-diffusion coefficient. We ran simulations using a time steps of 1, 0.5, 0.25 and 0.1 fs and calculated

the self-diffusion coefficient for each simulation. However, once again the differences between the calculated self-diffusion coefficients were negligible. This raised the question of whether gradients of the VMM were being properly calculated.

Temperature of Maximum Density, Expansivity and Compressibility

The properties of temperature of maximum density (T_{md}), expansivity and compressibility were simulated by running multiple simulations using NVT with different box sizes. These simulations were used to generate a pressure vs. density relationship to predict the box density under atmospheric pressure. This method was first tested using TIP4P/2005. Figure 4 shows one such pressure vs. density relationship at 300 K.

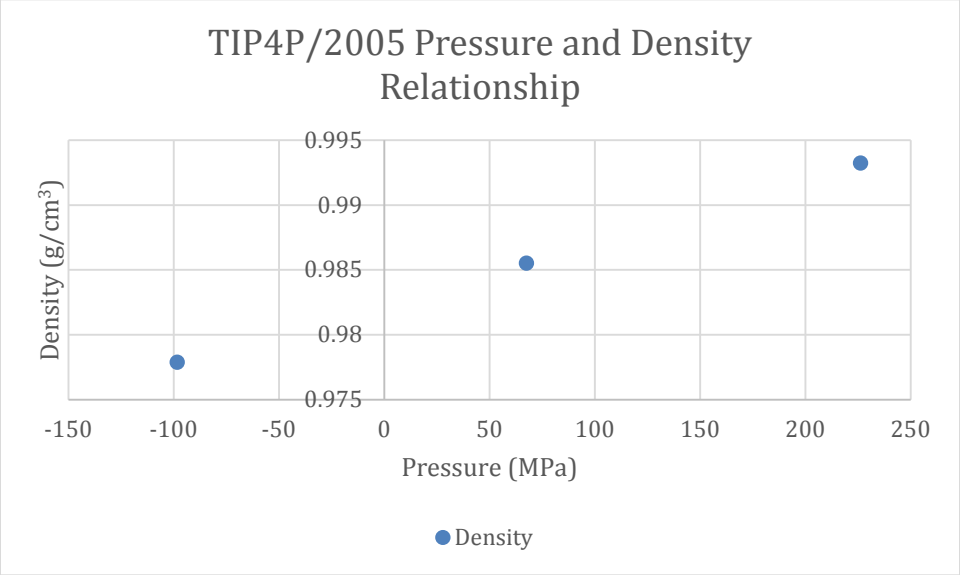

Figure 4 – MD simulation relationship between ensemble pressure and box density for the TIP4P/2005 potential. Note how linear the ensemble pressure vs box density relationship is for this potential.

The water densities of 1 bar pressure were calculated using linear relationships, like the one seen in Figure 4, for twelve different temperatures using TIP4P/2005 (Figure 5). The following expression was used to calculate the maximum density (Taken from Abascal and Vega 2005):

$$\rho = a + \frac{b}{T} + \frac{c}{T^2} + \frac{d}{T^3} + \frac{e}{T^4} + \frac{f}{T^5} \quad (33)$$

The coefficients of the fit were a = 0.3164, b = 381.4, c = -5.318x10^4, d = -539.1, e = 0.5211, f = 0.2316. The expression gives a reproduced T_{md} of 279 K for the TIP4P/2005 potential, compared to the literature TIP4P/2005 T_{md} of 278 K.

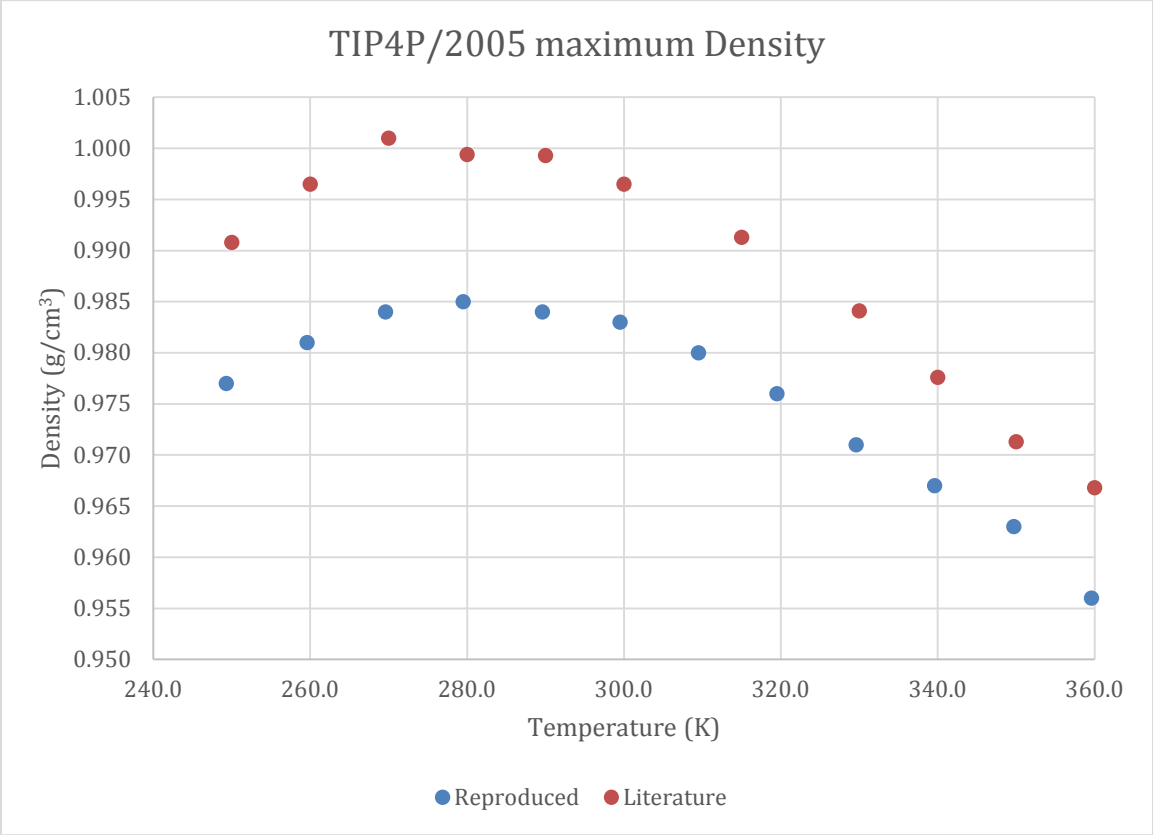

Figure 5 – Comparison of the reproduced with the literature TIP4P/2005 density values over a suite of temperatures. The T_{md} predicted by the reproduced curve differed from the literature T_{md} by 1 K.

The thermal expansion coefficient (expansivity) α_p is defined as:

$$\alpha_p = -\frac{1}{V}\left(\frac{\partial V}{\partial T}\right)_P \quad (34)$$

Following the method of Abascal and Vega (2005), the expansivity for the TIP4P/2005 potential was obtained by analytical differentiation of the polynomial fit used to determine the maximum density. Figure 6 shows the results of the expansivity

reproduced here as well as the Abascal and Vega (2005) reported values for TIP4P/2005. The average deviation of the reproduced values from the literature values was 5%.

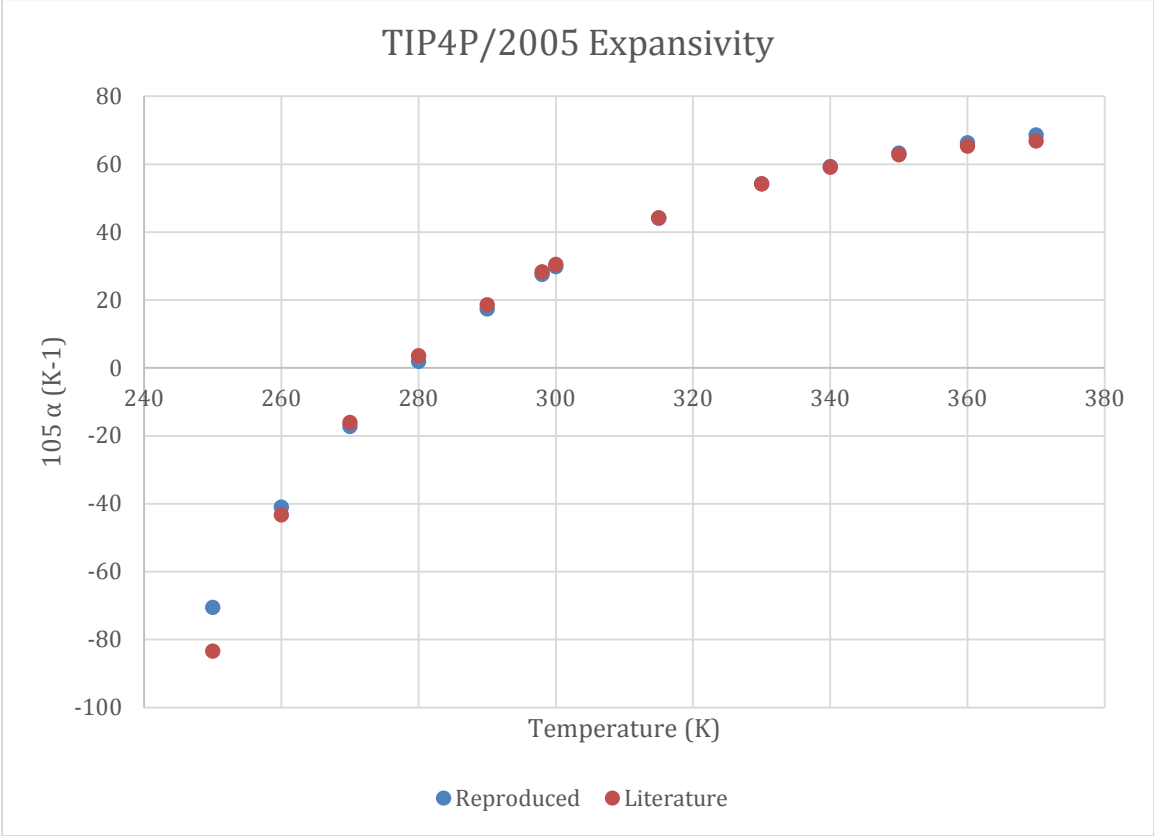

Figure 6 – Comparison of the reproduced with the literature TIP4P/2005 expansivity values over a suite of temperatures. The average deviation from the literature values was 5%.

The isothermal compressibility is defined as:

$$\kappa_T = -\frac{1}{V}\left(\frac{\partial V}{\partial p}\right)_T \tag{35}$$

The partial derivative of volume with respect to pressure at constant temperature was calculated using a 2nd order polynomial. A comparison of the estimated Abascal and Vega (2005) compressibility values with the TIP4P/2005 potential values reproduced here is provided in Figure 7. The average deviation from the literature values was about 6%.

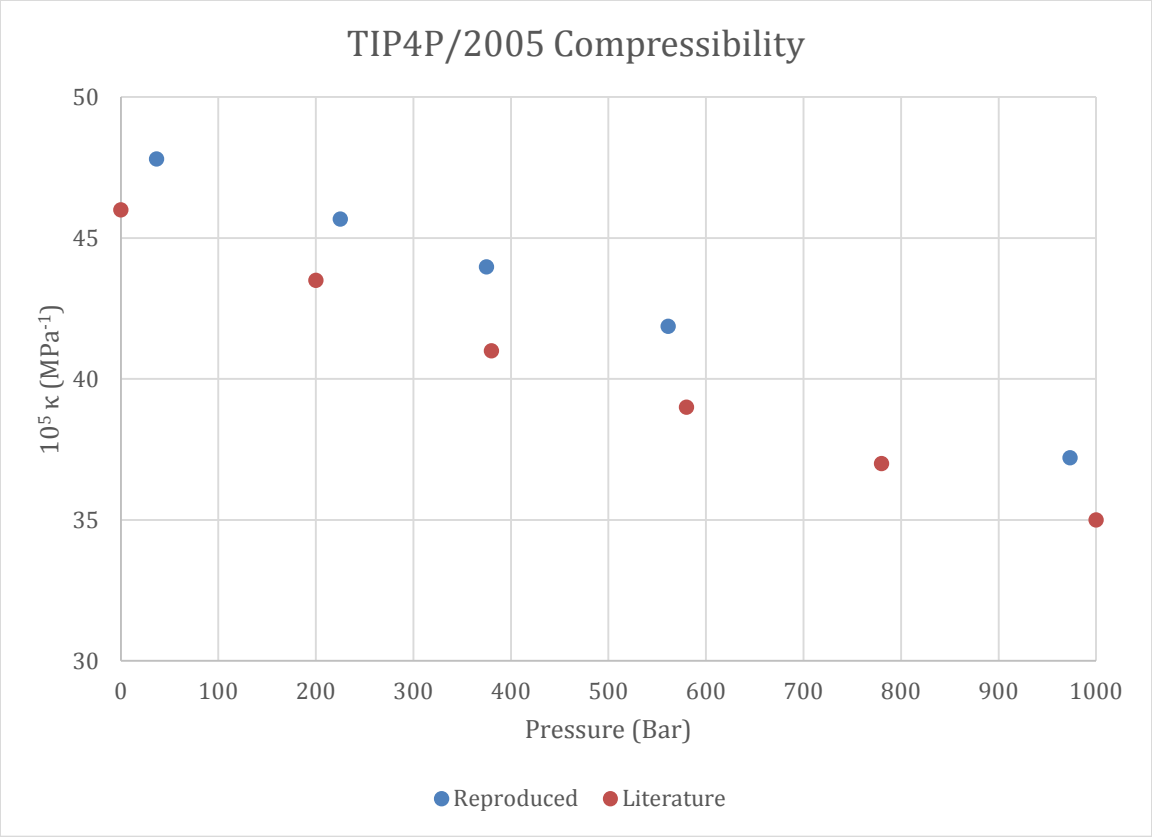

Figure 7 – Comparison of the reproduced with the literature TIP4P/2005 compressibility values over a suite of temperatures. The average deviation from the literature values was about 6%.

To test the VMM's simulated maximum density, expansivity and compressibility, we used the above methodology. Therefore, we started by calculating pressure vs. density relationships for ten different temperatures. However, unlike TIP4P/2005, the VMM simulations did not produce a linear relationship between pressure and density for any of the tested temperatures. To verify that the simulations were properly equilibrated, we decided to calculate the standard deviations of the simulations' ensemble pressures. We did this by re-running several simulations multiple times. The re-run simulations were chosen such that we sampled a good spread over box density and temperature. We used the re-run ensemble pressures to calculate a standard deviation of the pressure for each of the selected re-run simulations. All but one of the ensemble pressures exhibited standard

deviations between 1-5%. This suggests that the simulations were sufficiently equilibrated. Figure 8 shows one such pressure vs. density relationship while Table 2 compares the linearity of the pressure vs density relationship for the VMM and TIP4P/2005 simulations at various temperatures. Because of the combined failures of all the above tests, we greatly suspected the gradients of the model were being improperly calculated. We therefore performed a simulation using the NVE ensemble to test this hypothesis.

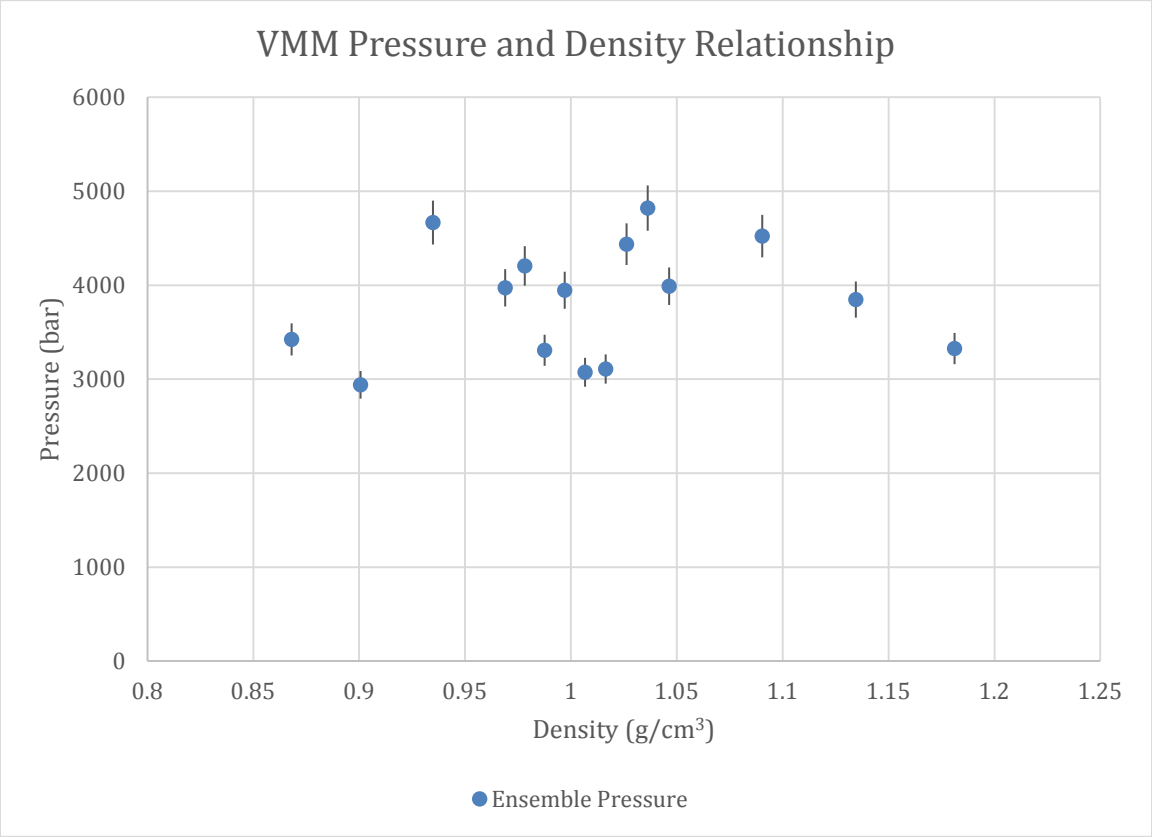

Figure 8 – MD simulation relationship between ensemble pressure and box density for the VMM OH potential. Notice how there is no discernable relationship between box density and ensemble pressure.

Temperature (K)	TIP4P/2005 R^2	VMM R^2
260	0.9967	0.2928
270	0.9993	0.1423
280	0.9837	0.1192
290	0.9984	0.4315
300	0.9998	0.0182
310	0.9970	0.3742
320	0.9973	0.2425
330	0.9999	0.6279
340	0.9998	0.2870
350	0.9998	0.2546

Table 2 – Comparison of the linearity for the ensemble pressure-box density relationship between the VMM OH and the TIP4P/2005 potentials over a suite of temperatures. Note how the relationship for the VMM OH potential is non-linear for all sampled temperatures.

Energy Conservation

We performed a simulation using the NVE ensemble to determine if the gradients of the VMM OH potential were being improperly calculated. The simulation was equilibrated to a temperature of 298 K over 1 ps using the NVT ensemble. Figure 9 shows the potential energy during the NVE portion of the simulation. The observed energy gain confirmed our hypothesis that the gradients of the VMM were being improperly calculated. Furthermore, the energy gain, and subsequent temperature increase, also explained the gas-phase-like self-diffusion coefficient we measured. We reasoned that if there existed any discontinuities in the VMM's potentials, these would cause the observed energy gain. We therefore decided to systematically examine the valence monopole and dipole potentials to determine if there existed any discontinuities in these potentials.

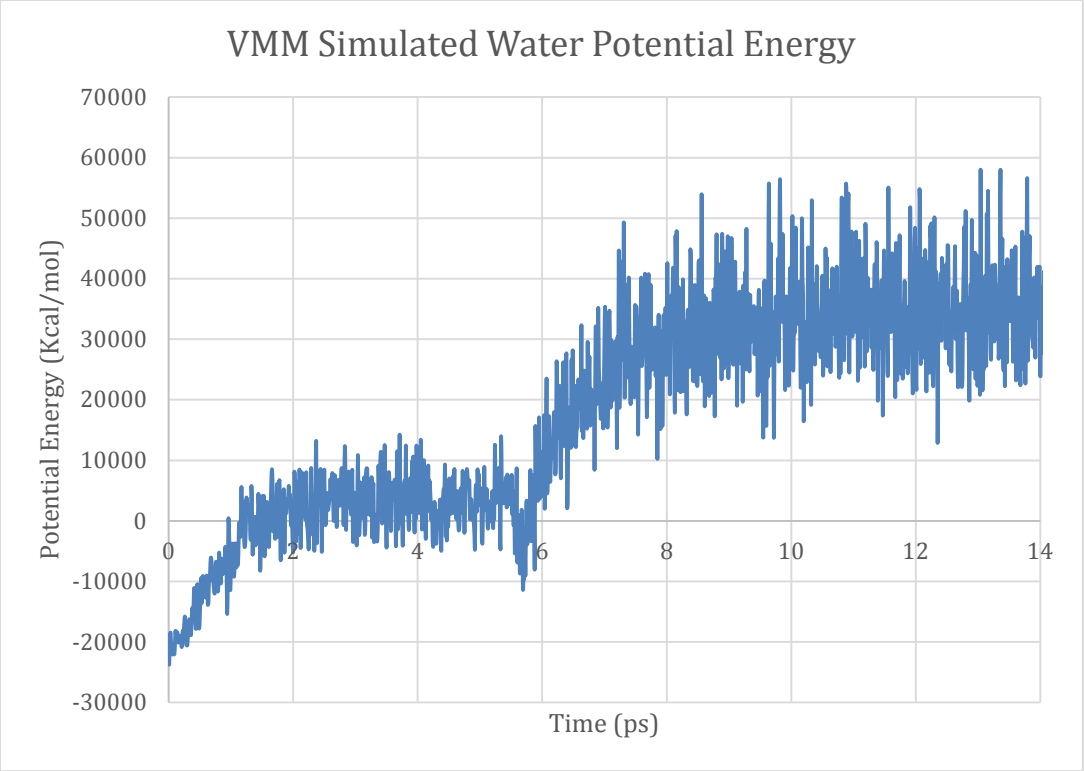

Figure 9 – MD simulation box potential energy using the VMM OH potential. The increase in energy over time evidences that the gradients of the VMM are being improperly calculated.

Valence Monopole and Dipole Potentials

Here we examine the valence monopole (two-body) and valence dipole (three-body) potentials of the VMM. We did this to determine if any discontinuities existed in these potentials, which would account for the lack of energy conservation. We found one significant discontinuity in the valence monopole potential for a strong oxygen-hydrogen bond. We added a smoothing function to the discontinuity and performed a second simulation again using the NVE ensemble. The energy conservation in this second simulation improved considerably, however the problem of energy gain remained. Therefore, we suspect there may yet exist discontinuities in the transitions between ideal states of the VMM.

Valence Monopole Potentials

Here we examine the two-body potentials of the VMM's OH potential. We first present the repulsive, Morse-cut potentials for the hydrogen-hydrogen and oxygen-oxygen pairs. Next, we examine a strong oxygen-hydrogen bond potential by pulling apart a hydroxide ion. Finally, we examine the weak oxygen-hydrogen bond potential by pulling apart a water trimer arranged in a tetrahedral configuration.

Figures 10 and 11 present the Morse-cut potentials for two hydrogen ions and two oxygen ions, respectively. The HH Morse-cut potential was particularly suspect because, as previously noted, during MD simulation the hydrogen atoms preferentially oriented themselves towards each other rather than towards neighboring oxygens. Despite this unusual structuring, the Morse-cut potential for neither hydrogen nor oxygen ions show any anomalous behavior.

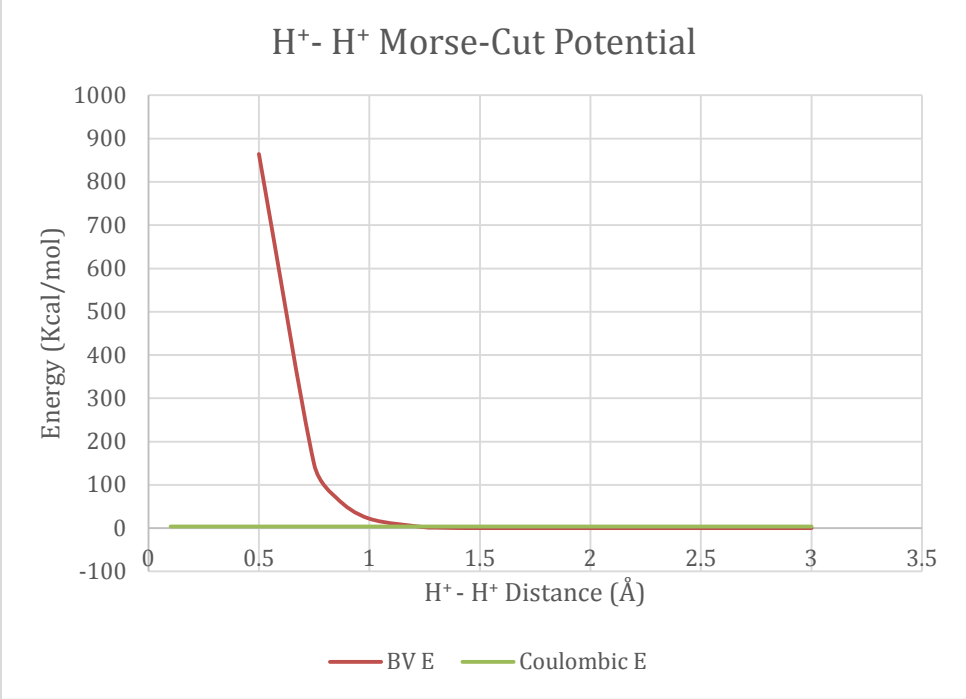

Figure 10 – Morse-cut and soft-core Coulombic potential curves for two H^+ ions. The coulombic potential is nearly flat because the radius of curvature of the potential curve is very small. Note how there is no discontinuity in the potential curve.

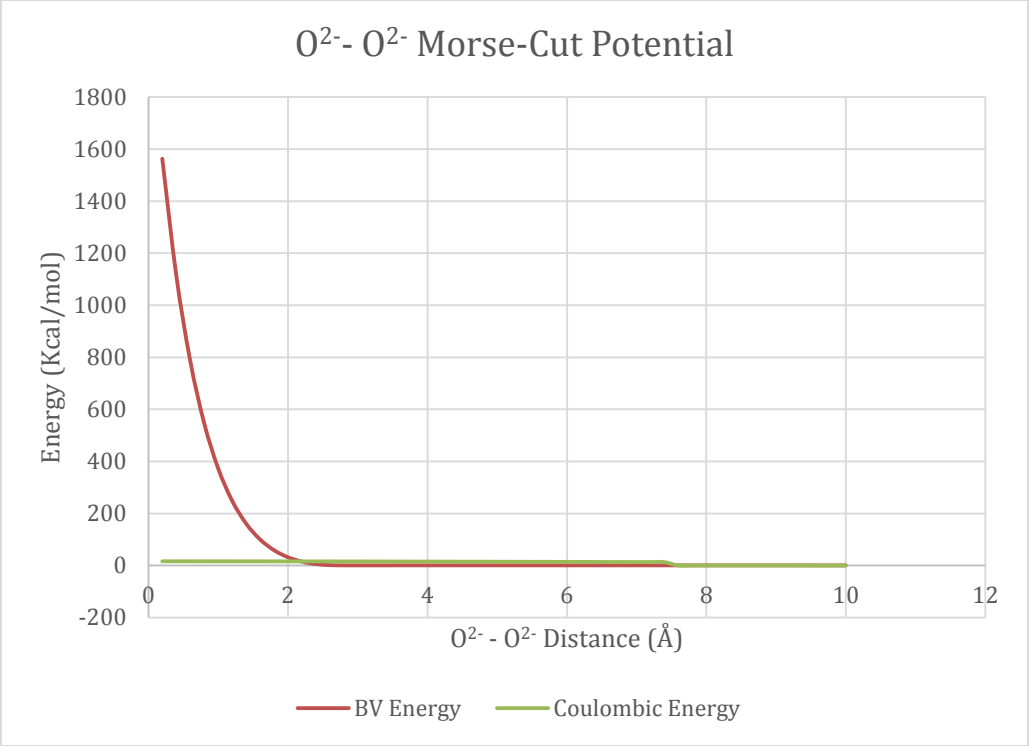

Figure 11 – Morse-cut and soft-core Coulombic potential curves for two O^{2-} ions. The coulombic potential is nearly flat because the radius of curvature of the potential curve is very small. Note how there is no discontinuity in the potential curve.

Figure 12 shows the valence monopole potential for a strong oxygen-hydrogen bond. The potential curve exhibits a significant discontinuity at 3 Å. This sharp cutoff was sufficient for the VMM OH potential as an equilibrium energy model, but posed a severe problem for a potential designed for use in MD simulation. Therefore, a smoothing function was applied to the cutoff, producing a new curve (Figure 13).

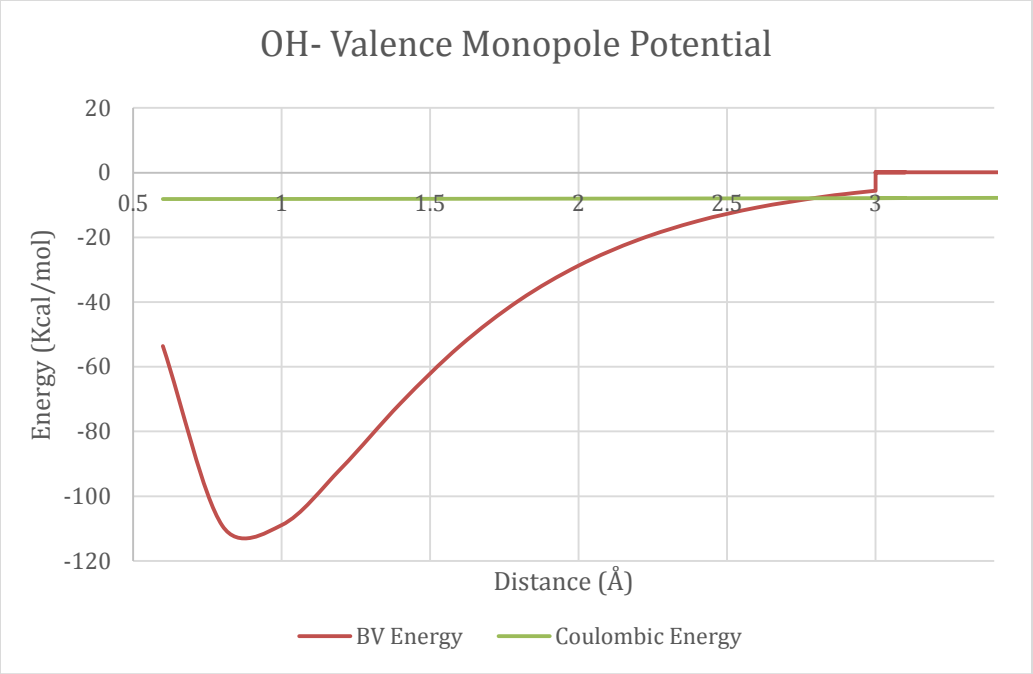

Figure 12 – Valence monopole and soft-core Coulombic potential curves of a hydroxide ion (OH-). The coulombic potential is nearly flat because the radius of curvature of the potential curve is very small. Note the valence monopole potential curve discontinuity at 3 Å bond length.

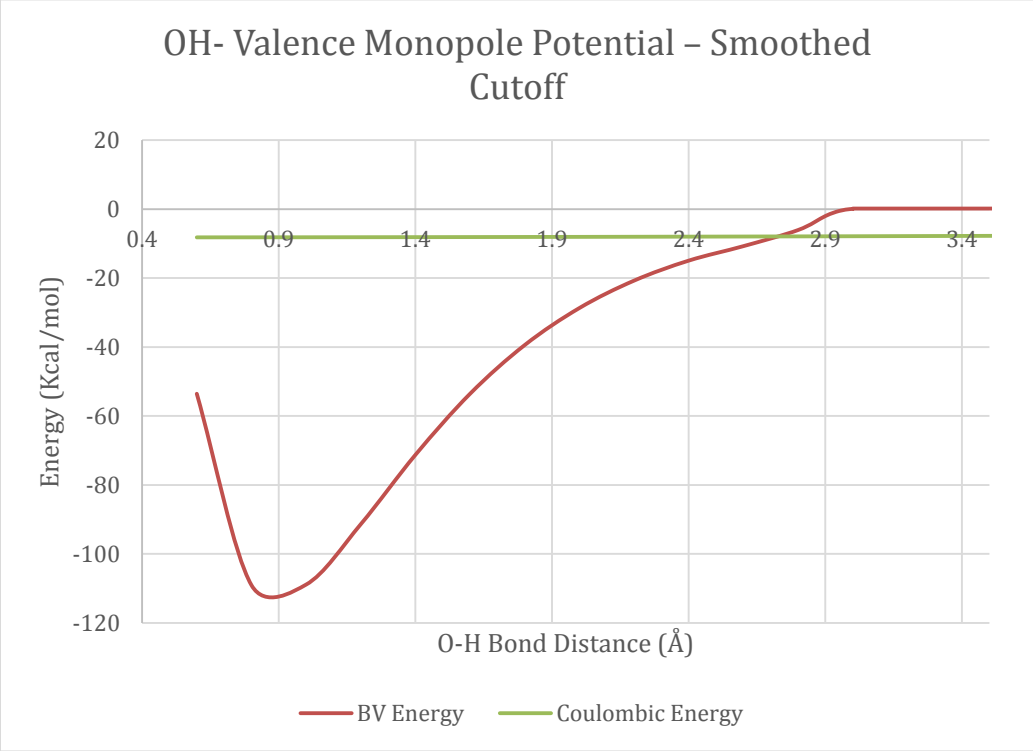

Figure 13 – Valence monopole and soft-core Coulombic potential curves of a hydroxide ion (OH-). Note how the valence monopole potential curve discontinuity has been smoothed.

After adding the smoothing function to the strong oxygen-hydrogen bond potential, we performed a follow-up simulation using the NVE ensemble to see if the gradients would calculate properly. Unfortunately, this follow-up simulation did not conserve energy, indicating there may still exist discontinuities in some other portion of the VMM OH potential. However, significant changes were observed after smoothing the cutoff. Table 3 shows ensemble averaged values, averaged over 11 ps, obtained from the initial and follow-up simulations performed using the NVE ensemble.

Model State	Temperature (K)	Pressure (Mpa)	Energy (Kcal/mol)
Pre-Smoothing	221929.9825	3088278.106	34971.12872
Post-Smoothing	1918.388427	24846.90634	-16637.77909

Table 3 – Comparison of MD simulation ensemble averages using temperature, pressure, and total energy using the VMM OH potential before and after smoothing the valence monopole potential curve discontinuity, as observed in Figures 12 and 13. These ensemble averages were obtained using the NVE ensemble. Notice the significant improvements in the values of the averages after the addition of the smoothing function.

We last examined the valence monopole potential for a weak oxygen-hydrogen bond. Because the structure of water is tetrahedral, we generated a water trimer with two neighboring water molecules in a tetrahedral configuration around the central water (Figure 14).

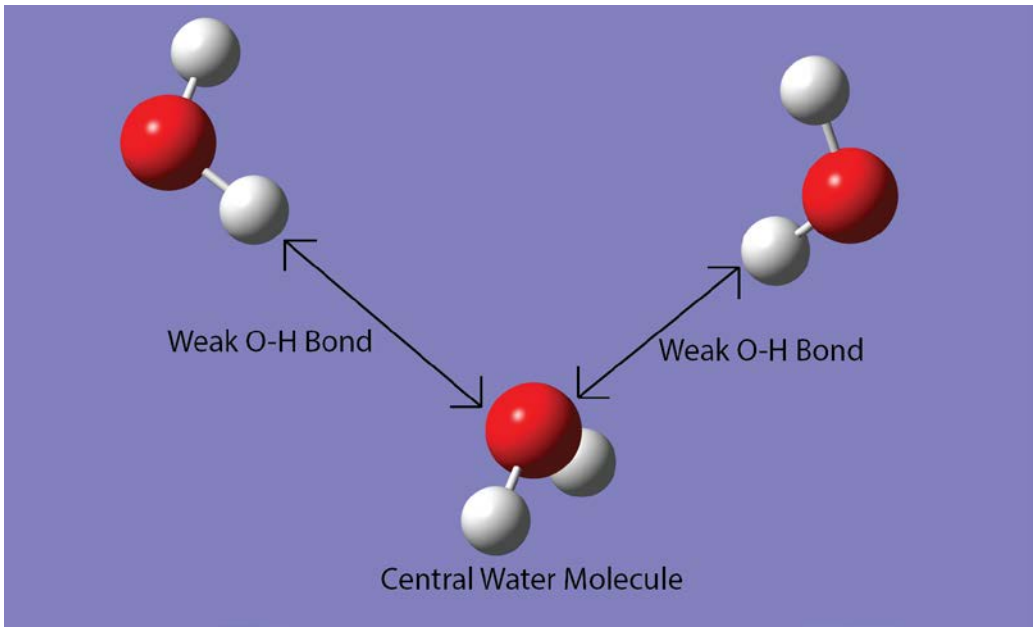

Figure 14 – Water trimer configuration used to generate the 3D potential energy surfaces seen in Figures 15 and 16.

We then obtained a potential energy surface by separately adjusting the bond lengths of each weak H-O bond from 0.6 Å to 3.1 Å in increments of 0.1 Å (Figure 15).

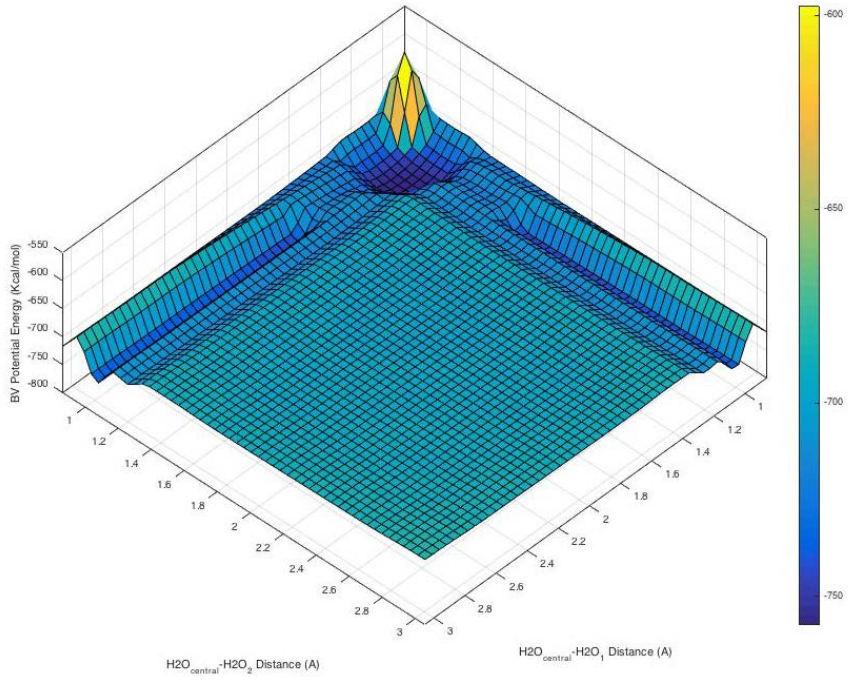

Figure 15 – Potential energy surface of two weak oxygen-hydrogen bonds (see Figure 14 for the molecular configuration). The weak hydrogen-oxygen bonds were adjusted in increments of 0.1 Å. Note the problematic energy wells between 1.4 Å – 0.8 Å.

The energy well observed around O-H distances from about 0.8 Å to 1.4 Å is the result of Eqn. 25 failing to predict the ideal coordination number for the approaching hydrogen. It is possible the rounding function of Eqn. 25 was not working properly, which allowed non-integer coordination numbers. Ultimately, the model allows the approaching hydrogen atom to become "bonded" to both oxygen atoms. Thus, we developed Eqns. 28 and 29 to ensure that this "overbonding" problem can no longer occur.

We also decided that we needed to begin simplifying the model to ensure we could locate the VMM's remaining issues. This involved removing the soft-core electrostatics and extending the Morse-cut potential to include charged oxygen-hydrogen pairs. We replaced the soft-core electrostatics with traditional electrostatics and re-fit the short-range bond valence parameters accordingly. After extending the Morse-cut potential to include oxygen-hydrogen pairs, we reperformed the tetrahedral potential energy scan (as seen in Figure 15) to obtain a new surface (Figure 16). Figure 16 demonstrates that expanding the Morse-cut to include oxygen-hydrogen pairs successfully simplified these previously-complex interactions.

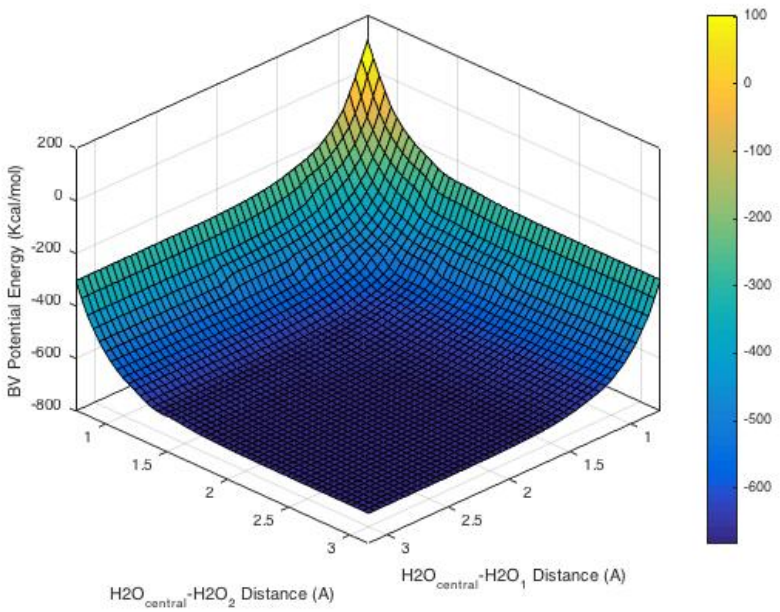

Figure 16 – Potential energy surface of two weak oxygen-hydrogen bonds (see Figure 14 for the molecular configuration). The weak hydrogen-oxygen bonds were adjusted in increments of 0.1 Å. Note how the potential is simple and purely repulsive.

Valence Dipole Potential

Here we present the three-body valence dipole potential for a water molecule. As previously noted, examination of the HOH bond angles during MD simulation revealed a wide distribution of bond angles. We therefore decided to examine the HOH valence dipole potential for discontinuities (Figure 17). However, we found no discontinuities in this potential. We therefore concluded that the valence dipole moment introduced too much angular flexibility, which allowed for the wide distribution of HOH bond angles. We also suspect that this angular flexibility is responsible for the incorrect water structure observed in the RDFs presented above. However, how to adjust the valence dipole potential to fix this issue was unclear because it is already a very simple potential: it uses a simple harmonic function and has only one ideal value. Ultimately, the angular

flexibility issue was resolved by turning off the electrostatic interactions between hydrogen ions bound to the same oxygen.

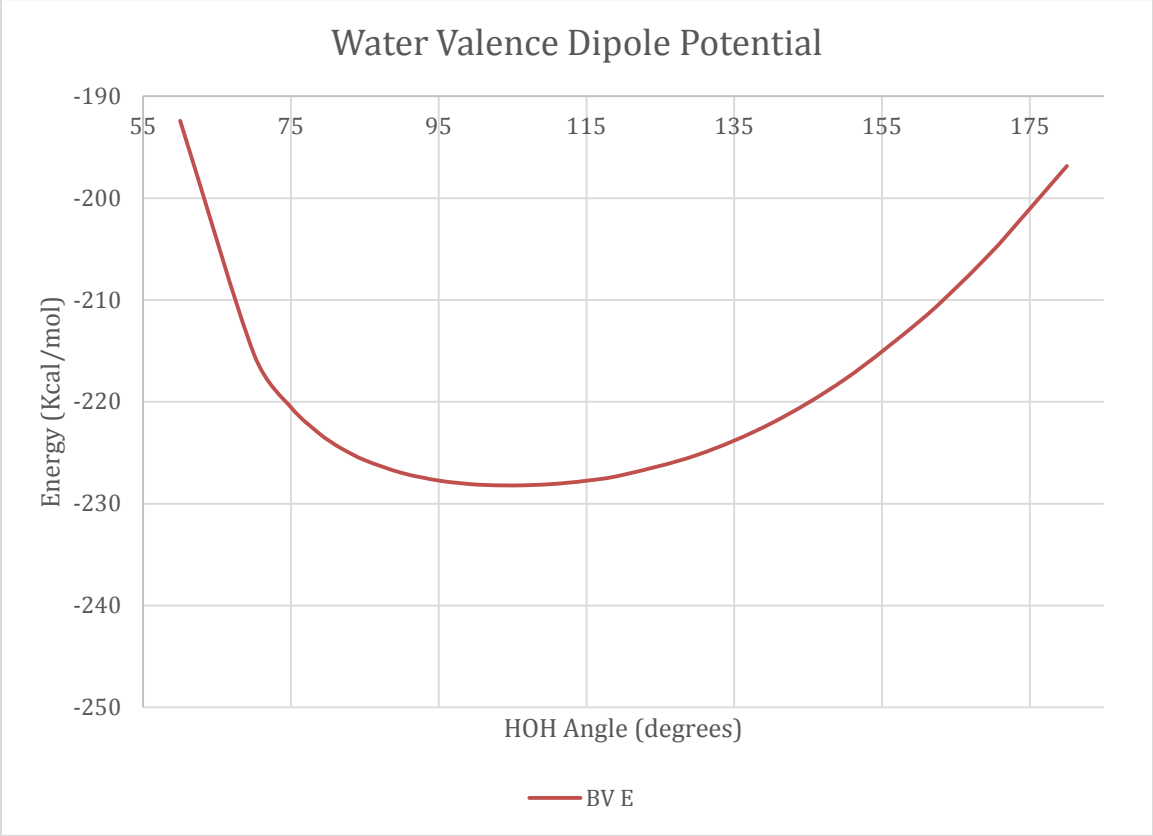

Figure 17 – Valence dipole potential curve for a water molecule. Note how the curve is a simple harmonic potential with no discontinuities.

CONCLUSIONS

Both the success of the equilibrium energy model and the quality of the *ab initio* data used to augment the fitting set of the VMM's parameters indicate that adapting the parameterization of the VMM to a reactive MD potential is highly plausible. We still believe it is possible to adapt the VMM to a reactive MD potential, however the tests discussed above indicate there are still significant problems with the model itself. For example, we suspect transitions between the integer values of N_{coord} (Eqn. 25) may be creating discontinuities in the valence monopole and dipole potentials of the VMM,

which discontinuities cause the gradients to calculate improperly. Ultimately, we identified two major causes for the observed issues with the VMM. First, our parameterization is new; therefore, no prior work has been done to adapt it to an MD force field. Second, our parameterization is rather complex due to the multibody nature of the valence monopole and dipole potentials, which can make sourcing the identified issues very challenging. Therefore, it is likely that further simplification of the model will yet be necessary to uncover and source the remaining issues associated with the model.

One way to simplify the model may be to use a smaller fitting set for the VMM's parameters. Included in the fitting set (Appendix – Tables 3 and 4) were many highly unusual, or even theoretical, molecules. It is likely that accounting for these strange, or even non-existent, molecules introduced an elevated level of complexity into the model. Therefore, it may be necessary to remove some of these unusual molecules from the fitting set and recalibrate the model to a smaller but simpler data set. Once the model has been adequately simplified, other outstanding issues such as energy conservation and long-range structure should be much easier to both find and resolve.

REFERENCES CITED

Abascal, J. L. F. and C. Vega (2005). "A General Purpose Model for the Condenses Phases of Water: TIP4P/2005." J. Chem. Phys. **123**.

Aryanpour, M., et al. (2010). "Development of a Reactive Force Field for Iron-Oxyhydroxide Systems." J. Phys. Chem. A **114**: 6298-6307.

Badger, R. M. (1934). "A Relation Between Internuclear Distances and Bond Force Constants." The Journal of Chemical Physics **2**: 128-131.

Balabanov, N. B. and K. A. Peterson (2005). "Systematically convergent basis sets for transition metals. I. All-electron correlation consistent basis sets for the 3 d elements Sc–Zn." Journal of Chemical Physics **123**.

Ball, P. (2008). "Water an Enduring Mystery." NATURE **452**: 291-292.

Bernal, J. D. and R. H. Fowler (1933). "A Theory of Water and Ionic Solution, with Particular Reference to Hydrogen and Hydroxyl Ions." The Journal of Chemical Physics **1**.

Beutler, T. C., et al. (1994). "Avoiding singularities and numerical instabilities in free energy calculations based on molecular simulations." Chemical Physics Letters **222**: 529-539.

Bickmore, B. R., et al. (2013). "Electronic structure effects in the vectorial bond-valence model." American Mineralogist **98**(2-3): 340-349.

Billeter, S. R., et al. (1994). "Can the density maximum of water be found by computer simulation?" J. Chem. Phys. **100**(6692).

Brenner, D. W. (1990). "Empirical potential for hydrocarbons for use in simulating the chemical vapor deposition of diamond films." Physical Review B **42**: 9458-9471.

Brown, D. and D. Altermatt (1985). "Bond valence parameters obtained from a systematic analysis of the iorganic crystal structure database." Acta Crystallographica **41**: 244-247.

Brown, I. D. (2002). The Chemical Bond in Inorganic Chemistry: The Bond Valence Model. New York, Oxford University Press.

Burnham, C. J. and S. S. Xantheas (2002). "Development of transferable interaction models for water. I. Prominent features of the water dimer potential energy surface." J. Chem. Phys. **116**.

Chaplin, M. (2001). "Water Structure and Science." 2017.

Comba, P., et al. (2009). Molecular modeling of inorganic compounds. Weinheim, Wiley-VCH.

Cooper, V. R., et al. (2003). Extending first principles modeling with crystal chemistry: A bond-valence based classical potential. Fundamental Physics of Ferroelectrics. P. K. Davies and D. J. Singh. Melville, New York, American Institute of Physics**:** 220-230.

Cramer, C. J. (2004). Essentials of Computational Chemistry. Chichester, UK, Wiley.

Cramer, C. J. (2004). Essentials of computational chemistry : theories and models. Chichester, West Sussex ; Hoboken, NJ, J. Wiley.

Cygan, R. T., et al. (2004). "Molecular Models of Hydroxide, Oxyhydroxide, and Clay Phases and the Development of a General Force Field." The Journal of Physical Chemistry B **108**(4): 1255-1266.

Ewald, P. P. (1921). "Die Berechnung optischer und elektrostatischer Gitterpotentiale." Annalen der Physik **369**(3): 253-287.

Finney, J. L. (2001). "The Water Molecule and its Interactions: The Interaction between Theory, Modelling and Experiment." J. Mol. Liq. **90**.

Finnis, M. W. and S. J. E. (1984). "A simple empirical N-body potential for transition metals." Philosophical Magazine A **50**: 45-55.

Glättli, A., et al. (2002). "Derivation of an improved simple point charge model for liquid water: SPC/A and SPC/L." J. Chem. Phys. **116**.

Grinberg, I., et al. (2002). "Relationship between local structure and phase transitions of a disordered solid solution." Nature **419**: 909-911.

Grinberg, I., et al. (2004). "Oxide chemistry and local structure of $PbZr_xTi_{1-x}O_3$ studied by density-functional theory supercell calculations." Physical Review B **69**: 144118.

Grinberg, I., et al. (2009). "Molecular dynamics study of dielectric response in a relaxor ferroelectric." Physical Review Letters **103**: 197601.

Guillot, B. (2002). "A Reappraisal of What we have Learnt During Three Decades of Computer Simulations on Water." J. Mol. Liq. **101**.

H. Yu, T. H. and W. F. v. Gunsteren (2003). "Development of a simple, self-consistent polarizable model for liquid water." J. Chem. Phys. **118**.

Hinchliffe, A. (2003). Molecular Modelling for Beginners. Manchester, John Wiley & Sons Ltd.

Horn, H. W., et al. (2004). "Development of an improved four-site water model for biomolecular simulations: TIP4P-Ew." J. Chem. Phys. **120**.

Johnston, V. H. S. (1966). Gas Phase Reaction Rate Theory. New York, Ronald Press.

Jorgensen, W. L. and C. Jenson (1998). "Temperature dependence of TIP3P, SPC, and TIP4P water from NPT Monte Carlo simulations: Seeking a temperature of maximum density." J. Comp. Chem. **19**: 1179 - 1186.

Liu, H., et al. (2016). "Transferable ab Initio Dipole Moment for Water: Three Applications to Bulk Water." J. Phys. Chem. B **120**: 1735-1742.

Liu, S., et al. (2013). "Development of a bond-valence based interatomic potential for BiFeO3 for accurate molecular dynamics simulations." Journal of Physics: Condensed Matter **25**: 102202.

Liu, S., et al. (2013). "Reinterpretation of the bond-valence model with bond-order formalism: An improved bond-valence-based interatomic potential for $PbTiO_3$." Physical Review B **88**: 104102.

Mahoney, M. W. and W. L. Jorgensen (2000). "A five-site model for liquid water and the reproduction of the density anomaly by rigid, nonpolarizable potential functions." J. Chem. Phys. **112**.

Mason, P. E. and J. W. Brady (2007). "Tetrahedrality" and the Relationship between Collective Structure and Radial Distribution Functions in Liquid Water." J. Phys. Chem. B **2007**: 5669-5679.

Medders, G. R., et al. (2014). "Development of a "First- Principles" Water Potential with Flexible Monomers. Iii. Liquid Phase Properties." J. Chem. Theory Comput. **10**: 2906-2910.

Nada, H. and J. P. J. M. v. d. Eerden (2003). "An intermolecular potential model for the simulation of ice and water near the melting point: A six-site model of H2O." J. Chem. Phys. **118**.

Olano, L. R. and S. W. Rick (2005). "Fluctuating Charge Normal Modes: An Algorithm for Implementing Molecular Dynamics Simulations with Polarizable Potentials." J. Comput. Chem. **26**.

Pauling, L. (1929). "The principles determining the structure of complex ionic crystals." Journal of the American Chemical Society **51**: 1010-1026.

Peterson, K. A. and T. H. J. Dunning (2002). "Accurate correlation consistent basis sets for molecular core–valence correlation effects: The second row atoms Al–Ar, and the first row atoms B–Ne revisited." The Journal of Chemical Physics **117**.

Peterson, K. A. and C. Puzzarini (2005). "Systematically convergent basis sets for transition metals. II. Pseudopotential-based correlation consistent basis sets for the group 11 (Cu, Ag, Au) and 12 (Zn, Cd, Hg) elements." Theor Chem Acc **114**: 283-296.

Rappé, A. K. and C. J. Casewit (1997). Molecular mechanics across chemistry. Sausalito, CA, University Science Books.

Ren, P. and J. W. Ponder (2004). "Temperature and Pressure Dependence of the AMOEBA Water Model." J. Phys. Chem. B **108**: 13427– 13437.

Rowley, R. L. (1994). Statistical Mechanics for Thermophysical Property Calculations. Englewood Cliffs, New Jersey, Prentice-Hall.

Saint-Martin, H., et al. (2004). "An application of flexible constraints in Monte Carlo simulations of the isobaric–isothermal ensemble of liquid water and ice Ih with the polarizable and flexible mobile charge densities in harmonic oscillators model." J. Chem. Phys. **120**.

Shepherd, K., et al. (2016). "The Valence Quadrupole Moment." American Mineralogist **101**: 362-370.

Shin, Y.-H., et al. (2005). "Development of a bond-valence molecular-dynamics model for complex oxides." Physical Review B **71**: No. 054104.

Shin, Y.-H., et al. (2007). "Nucleation and growth mechanism of ferroelectric domain-wall motion." NATURE **449**: 881-884.

Shin, Y.-H., et al. (2008). "Order-disorder character of $PbTiO_3$." Journal of Physics: Condensed Matter **20**(1): 015224.

Takenaka, H., et al. (2013). "Anisotropic local correlations and dynamics in a relaxor ferroelectric." Physical Review Letters **110**(14): 147602.

Tan, M. L., et al. (2014). "The Molecular Charge Distribution, the Hydration Shell, and the Unique Properties of Liquid Water." J. Chem. Phys. **141**.

Tan, M. L., et al. (2016). "Molecular Multipole Potential energy functions for water." J. Phys. Chem. B. **120**: 1833-1842.

Te, J. A. and T. Ichiye (2010). "Temperature and Pressure Dependence of the Optimized Soft Sticky Dipole-Quadrupole-Octupole Water Model." J. Chem. Phys. **132**.

Tersoff, J. (1988). "New empirical approach for the structure and energy of covalent systems." Physical Review B **37**: 6991-7000.

Van der Spoel, D., et al. (1998). "A Systematic Study of Water Models for Molecular Simulation: Derivation of Water Models Optimized for Use with a Reaction Field." J. Chem. Phys. **108**.

Van Duin, A. C. T., et al. (1994). "Delft Molecular Mechanics: A New Approach to Hydrocarbon Force Fields Inclusion of a Geometry-dependent Charge Calculation." J. Chem. Soc. Faraday Trans. **90**(19): 2881-2895.

Van Duin, A. C. T., et al. (2001). "A Reactive Force Field for Hydrocarbons." J. Phys. Chem. A **105**: 9396-9409.

Van Duin, A. C. T., et al. (2003). "ReaxFFSiO Reactive Force Field for Silicon and Silicon Oxide Systems." J. Phys. Chem. A **107**: 3803-3811.

Van Duin, A. C. T., et al. (2014). "A Reaxff Reactive Force-field for Proton Transfer Reactions in Bulk Water and its Applications to Heterogeneous Catalysis, Computational Catalysis."

Vega, C., et al. (2005). "Radial distribution functions and densities for the SPC/E, TIP4P and TIP5P models for liquid water and ices Ih, Ic, II, III, IV, V, VI, VII, VIII, IX, XI and XII." Phys. Chem. Chem. Phys. **7**: 1450-1456.

Wallqvist, A. and B. J. Berne (1993). "Effective potentials for liquid water using polarizable and nonpolarizable models." J. Phys. Chem. **97**: 13841 - 13851.

Wander, M. C. F. and B. R. Bickmore (2016). "A preliminary valence-multipole potential energy model: Al-Si-H-O system." American Mineralogist **101**: 1862-1872.

Wander, M. C. F., et al. (2015). "The use of cation-cation and anion-anion bonds to augment the bond-valence model." American Mineralogist **100**: 148-159.

Wander, M. C. F., et al. (2015). "AIM Anaylsis and the form of the Bond-Valence Equation." American Mineralogist **100**: 160-171.

Wu, Y., et al. (2006). "Flexible simple point-charge water model with improved liquid-state properties." The Journal of Chemical Physics **124**.

Xantheas, S. S. (2005). "Interaction Potentials for Water from Accurate Cluster Calculations." Struc Bond **116**: 119-148.

APPENDIX

Theory	Core	Basis Set	Bond Length (Å)	Time (minutes)	Bond Length Error
CCSD	Full	aug-vqz	3.19	2.01	1.14E-01
CCSD	full	aug-cvdz	3.06	17.52	1.92E-02
CCSD	full	aug-cvtz	1.95	303.31	1.12E+00
CCSD	no full	aug-vtz	3.15	3.87	6.94E-02
CCSD	no full	aug-vdz	3.10	69.96	1.68E-02
CCSD	no full	aug-vdz*	3.20	0.61	1.25E-01
CCSD	no full	aug-vtz	3.20	0.50	1.25E-01
CCSD	no full	aug-vqz	3.18	3.86	9.88E-02
CCSD	no full	aug-cvdz	3.20	0.65	1.24E-01
CCSD	no full	aug-cvtz	3.18	6.83	9.88E-02
CCSD	no full	aug-vqz	3.18	118.63	9.84E-02
CCSD	no full	aug-cvdz	3.19	1.19	1.11E-01
CCSD	no full	aug-cvtz	3.18	36.95	9.91E-02
CCSD	Full	aug-vdz	3.1933	1.65	1.143E-01
CCSD	Full	aug-vtz	3.0595	13.95	1.950E-02
CCSD	Full	vdz	3.21	0.62	1.3E-01
CCSD	Full	vtz	3.08	3.71	1.1E-03
CCSD	Full	vqz	2.96	52.63	1.1E-01
CCSD	full	cvdz	3.16	1.36	8.3E-02
CCSD	full	cvtz	3.10	29.28	2.3E-02
CCSD	full	cvqz	3.09	531.84	1.4E-02
CCSD	no full	vdz	3.20	0.32	1.3E-01
CCSD	no full	vtz	3.18	1.50	9.9E-02
CCSD	no full	vqz	3.18	26.28	9.8E-02
CCSD	no full	cvdz	3.19	0.52	1.1E-01
CCSD	no full	cvtz	3.18	15.37	9.9E-02
CCSD	no full	cvqz	3.18	288.91	1.0E-01
CCSDT	Full	vdz	3.21	0.72	1.3E-01
CCSDT	Full	vtz	3.08	4.05	4.0E-03
CCSDT	Full	vqz	2.96	32.52	1.2E-01
CCSDT	full	v5z	3.18	256.79	9.9E-02
CCSDT	full	cvdz	3.16	2.36	8.2E-02
CCSDT	full	cvtz	3.10	26.17	2.0E-02
CCSDT	full	cvqz	3.09	323.78	9.3E-03
CCSDT	full	cv5z	3.08	4513.37	1.0E-03
CCSDT	no full	vdz	3.20	0.41	1.3E-01
CCSDT	no full	vtz	3.18	1.10	9.9E-02

CCSDT	no full	vqz	3.18	15.05	9.8E-02
CCSDT	no full	v5z	3.18	68.67	9.9E-02
CCSDT	no full	cvdz	3.19	0.55	1.1E-01
CCSDT	no full	cvtz	3.18	6.74	9.9E-02
CCSDT	no full	cvqz	3.18	69.02	1.0E-01
CCSDT	no full	cv5z	3.18	590.02	1.0E-01
CID	Full	vdz	3.21	0.37	1.3E-01
CID	Full	vtz	3.08	2.05	1.8E-03
CID	Full	vqz	2.97	29.94	1.1E-01
CID	full	cvdz	3.14	0.65	6.3E-02
CID	full	cvtz	3.09	14.82	1.4E-02
CID	full	cvqz	3.09	256.83	9.3E-03
CID	no full	vdz	3.20	0.28	1.3E-01
CID	no full	vtz	3.18	1.20	9.9E-02
CID	no full	vqz	3.18	16.66	9.8E-02
CID	no full	cvdz	3.19	0.41	1.1E-01
CID	no full	cvtz	3.18	12.12	9.9E-02
CID	no full	cvqz	3.18	159.17	1.0E-01

Appendix Table 1 – Test of various ab initio methods using Na_2.

Theory	R (Å)	De (kJ/mol)	Force Constant (k)	R Error (Å)	% Error k	% Error De	Time (s)
CCSD/cvdz	3.162	157.052	96.366	0.083	6.64%	107.3%	348.9
CCSD/cvtz	3.103	167.674	105.641	0.024	2.34%	121.3%	3030.2
CCSD/cvqz	3.093	132.882	104.663	0.014	1.40%	75.4%	34888.9
CCSD(t)/cvdz	3.161	133.643	95.441	0.082	7.54%	76.4%	561.5
CCSD(t)/cvtz	3.099	122.563	103.505	0.020	0.28%	61.8%	5173.6
CCSD(t)/cvqz	3.088	95.434	102.521	0.009	0.68%	26.0%	51746.5
CCSDT/cvdz	3.161	138.469	95.398	0.082	7.58%	82.8%	458.8
CCSDT/cvtz	3.099	124.206	103.548	0.020	0.32%	64.0%	4173.9
CCSDT/cvqz	3.088	95.434	102.521	0.009	0.68%	26.0%	42380.3

Appendix Table 2 – Ab initio bond scan tests using Na_2.

Molecule	R (Å)	Bond Valence (v.u.)	De (kJ/mol)	Force Constant (K)
2H2O	1.956	0.016	17.915	99.722
H2O OH-	1.217	0.287	129.360	1141.312
H2O OH-	1.215	0.290	126.916	1153.058
H5O2+	1.201	0.309	220.728	2153.211
H5O2+	1.181	0.337	220.728	2153.211
OH+	1.029	0.695	314.540	3286.532

H2O-	1.008	0.775	101.424	2637.204
H2O+	1.000	0.807	376.399	3933.573
H3O+	0.977	0.911	901.325	6592.694
OH	0.970	0.944	435.042	4721.048
OH-	0.967	0.959	363.461	4473.736
2H2O	0.964	0.976	132.699	1141.094
H2O2	0.963	0.981	432.905	4880.260
H2O	0.958	1.005	481.197	5118.829

Appendix Table 3 – Ab initio database for O-H interactions

Molecule	R (Å)	Bond Valence (v.u.)	De (kJ/mol)	Force Constant (K)
O2++	1.048	2.971	705.673	13766.636
O2+	1.118	2.503	683.930	10444.992
HOO+	1.198	2.055	620.713	7287.767
O2	1.210	1.998	609.994	7167.061
O3	1.271	1.717	287.453	3124.834
F2O2	1.295	1.622	289.272	3144.609
O2-	1.342	1.441	401.294	3714.691
Cl2O2	1.392	1.274	267.671	2427.469
Br2O2	1.388	1.286	287.453	2463.634
CH3OOCH3	1.445	1.117	331.016	2773.073
BH2OOBH2	1.450	1.104	276.977	2534.183
H2O2	1.455	1.089	321.858	2757.314
HOO-	1.509	0.952	321.971	2188.496
Li2O2	1.565	0.829	342.261	1801.297
Na2O2	1.581	0.796	229.110	1553.394

Appendix Table 4 – Ab initio database for O-O interactions